The ~~importance~~ influence of plant-water stress on vegetation-atmosphere exchanges: implications for ~~predictions of ground-level~~ ozone ~~in a warm world~~modelling

Tamara Emmerichs[1,3] , Yen-Sen Lu[2,3], and Domenico Taraborrelli[1,3]

[1]Institute of Energy and Climate Research, IEK-8: Troposphere, Forschungszentrum Jülich GmbH, Jülich, Germany
[2]Jülich Supercomputing Centre, Forschungszentrum Jülich GmbH, 52425 Jülich, Germany
[3]Center for Advanced Simulation and Analytics (CASA), Forschungszentrum Jülich GmbH, Jülich, Germany

Correspondence: Tamara Emmerichs (t.emmerichs@fz-juelich.de)

Abstract. Evapotranspiration is important for Earth~~'~~'s water and energy cycles as it strongly affects air temperature, cloud cover and precipitation. Leaf stomata are the conduit of transpiration. Thus, their opening is sensitive to weather and climate conditions. This feedback can exacerbate heat waves and can play a role in their spatio-temporal propagation. ~~Hence, the plant response to available water is a key element mediating vegetation-atmosphere interactions.~~

Sustained high temperatures strongly favor high ozone levels with significant negative ~~effects~~ impacts on air quality and thus human health. Our study ~~assesses~~ evaluates the process representation of evapotranspiration in the atmospheric chemistry model ECHAM/MESSy. ~~Diverse water stress parametrizations~~ Different water stress parametrisations are implemented in a stomatal model based on CO_2 assimilation. The stress factors depend on either soil moisture or leaf water potential ~~acting on~~ and action photosynthetic activity, mesophyll and stomatal conductance. The new functionalities reduce the initial overestimation of evapotranspiration in the model globally by more than ~~one order~~ an order of magnitude which is most important in the Southern Hemisphere. The intensity of simulated warm spells over continents is significantly ~~enhanced~~improved. For ozone, we find that a realistic model representation of plant-water stress ~~depresses~~ suppresses uptake by vegetation and enhances its photochemical production in the troposphere. These effects lead to ~~a general increases~~ an overall increase in simulated ground-level ozone which is most pronounced in the Southern Hemisphere over the continents. More sophisticated land surface models with multi-layer soil schemes could address the uncertainties ~~for~~ in representing plant dynamics representation due to too shallow roots . In regions with low evaporative loss but the representation of precipitation remains the largest uncertainty.

1 Introduction

The response of plants to water availability is crucial for climate models ~~since~~ because it determines the plant activity ~~driving~~ which drives photosynthesis and transpiration over vegetated land surface. Besides evaporation from open water and soil surfaces, ~~transpiration by plants is with 60-75 %~~ plant transpiration is the main contributor to evaporation and transpiration (*ET*: water returned ~~from land~~ to the atmosphere ~~) (Seneviratne et al., 2010). Its strength~~ from the land) (Seneviratne et al., 2010) with 60-75 % . Its magnitude depends on vegetation ~~coverage~~cover, surface wetness, and the availability of soil water for ~~vegetation root uptake~~ root uptake by vegetation roots for transpiration. Evapotranspiration (often ~~also termed~~ referred to as terrestrial evaporation, *ET*) in turn has multiple impacts on the hydrological, energy and biogeochemical cycles (Sellers et al., 1997; Seneviratne et al., 2010; Vicente-Serrano et al., 2022; Wang and Dickinson, 2012). A decrease ~~of~~ in *ET* in response to land drying reduces the flux of latent heat to the atmosphere. This leads to ~~increased~~ an increase in air temperature and ~~decreases~~ reduces the likelihood of ~~rainfall~~ precipitation (e.g., Seneviratne et al., 2010).

A ~~scarcity~~ shortage of soil water (water ~~lower than~~ below a critical threshold) ~~strengthens the physical plant-water stress~~ increases the physical water stress on the plant, limiting the transpiration ~~mediated by~~ through the stomata (~~plants'~~ plant pores). The resulting change in latent heat flux (of ~~vaporization~~evaporation, λ) ~~decreases~~ reduces the likelihood of rainfall (Miralles et al., 2019). These conditions, which are predicted to increase due to climate change, could potentially ~~amplify droughts and heatwaves (Kala et al., 2016). Thus, the water availability of plants is~~ increase droughts and heat waves (Kala et al., 2016). Plant water availability is therefore a key to ~~represent~~ the representation of such weather extremes in the Earth system models (e.g. review by Miralles et al. (2019)). In particular, ~~heatwaves~~ heat waves are projected to increase under climate change. Thus, the land-atmosphere coupling ~~gains in importance~~ becomes more important (Domeisen et al., 2022). Furthermore, terrestrial energy fluxes have become even more sensitive to vegetation ~~over the last~~ in recent decades as Forzieri et al. (2020) found in an observational data set from 1980 to 2016.

Most models use an empirical reduction factor dependent on soil moisture to represent the plant response to ~~dryness~~ drought (see review by Rogers et al. (2017)). However, this factor does not ~~simulate the plant response to dryness realistically~~ realistically simulate this. Instead, ~~parametrizations~~ parametrisations based on the independent leaf water potential (ψ) perform better (Verhoef and Egea, 2014). Leaf water potential is ~~a vital~~ an important variable to describe the plant's dependence on water, the chemical potential gradient from the root zone to the leaves (Klein, 2014; Sellers et al., 1997) and e.g. Paço et al. (2013) define it as one of the most reliable ~~plant-water~~ plant water stress indicators. The inclusion of ψ in stomatal models is consistent with the hypothesis that stomata regulate transpiration rates in order to avoid cavitation in the xylem. The water potential strongly modulates the stomatal conductance at the evaporating sites ~~within~~ in the leaf. This is a well established theoretical assumption for modelling transpiration (Tuzet et al., 2003, and references therein).

~~Yet, studies do not determine whether the plant-water stress acts on~~ However, studies have not determined whether the plant water stress affects photosynthesis or directly ~~modifies~~ alters the stomatal conductance, which depends on ~~the opening of the stomata~~ stomatal aperture (see reviews by De Kauwe et al. (2013); Rogers et al. (2017)). Thus, models differ ~~largely in this regard~~widely in this respect. Keenan et al. (2010) have shown that neglecting the water stress acting only on photosynthesis significantly ~~overestimate the stomatal opening~~overestimates the stomatal aperture. Applying the stress factor only to the stomatal conductance could not explain the observed reduction ~~of~~ in the assimilation rate in the plant. ~~Further~~Furthermore, measurement studies (Drake et al., 2018; Zhou et al., 2013; Egea et al., 2011; Keenan et al., 2010) agree that ~~the water stress acts on the stomata as well as~~ water stress affects both stomata and on non-stomatal processes in plants. ~~Thus, the sole~~

~~application of the water stress to the photosynthesisas done in e.g.~~ Therefore, applying water stress only to photosynthesis, as in the Community Land Model (CLM, Kennedy et al. (2019)), is not sufficient. Egea et al. (2011) has found that drought stress also has a detrimental effect on the mesophyll conductance, which regulates the diffusion between the ~~sub-stomatal internal cavities~~ internal stomata to the chloroplasts.

Tropospheric ozone is a major air pollutant that is harmful to both humans and plants. Its spatial and temporal evolution depends not only on emissions, but also crucially on meteorological variables such as temperature. In fact, the radical reactions that dominate the formation of O_3 are enhanced at high temperatures. Plant emissions of isoprene, an important ozone precursor, also respond strongly to increasing temperature, rising exponentially up to a temperature of 42°C (Guenther et al., 2006) . Both higher temperatures and drought inhibit dry deposition, an important sink for ozone and its precursors. Much of the dry deposition occurs at stomata during plant water/CO_2 exchange (transpiration/respiration). As plants close their stomata to limit the water loss (Katul et al., 2009), ozone uptake is greatly reduced.

We use the global atmospheric chemistry model ECHAM/MESSy ~~Atmospheric Chemistry (EMAC)~~(Modular Earth Submodel System), EMAC for short, (Jöckel et al., 2016) to investigate the multiple ~~feedbacks involved and~~ interactions involved and to assess the uncertainty ~~related to the evapotranspiration representation from land~~ associated with the representation of land evapotranspiration. This model is widely ~~applied to address the simulation and prediction of~~ used to simulate and predict atmospheric chemistry and ~~tackle~~ to address global air quality issues. As part of the Chemistry–Climate Model Initiative (CCMI) (Jöckel et al., 2016), the ~~model community also contributes~~ modelling community is also contributing to climate research. Here, we ~~explore multiple plant-water stress formulations regarding~~ investigate the uncertainties and variability ~~, firstly~~ of several plant water stress formulations, initially implemented in EMAC. We ~~assess~~ evaluate the performance of the different sensitivity studies ~~at global scale against~~ on a global scale using plant transpiration and evaporation data provided by the GLEAM model and the EUMETSAT satellite, respectively. ~~The consequences of changing the plant-water stress factor for ground-level air pollution are investigated in the next section~~To assess the impact of the different plant water stresses on ozone, we use a comprehensive chemistry with 310 reactions and 155 species in the gas phase. Anthropogenic emissions are prescribed from reanalysis and CCMI data. Natural emissions of ozone precursors (from lightning, soil and plants) are interactively simulated with corresponding measurements and parametrisations (Guenther et al., 2006; Tost et al., 2006; Kerkweg et al., 2006). We also assess the impact of a ~~changed plant-water~~ modified plant water response on evapotranspiration in a condition with 2xCO_2 state to account for the global warming. ~~This paper closes~~ The paper concludes with a general discussion of the approach and the model and a comprehensive summary of the results.

2 Methods

2.1 Model description

2.1.1 ~~Atmospheric model~~

We use the ECHAM/MESSy atmospheric chemistry model where MESSy (v2.55; Jöckel et al., 2010) provides a flexible infrastructure for coupling processes to build comprehensive Earth ~~system models~~ System Models (ESMs). This is ~~utilised~~ used here with the ~~fifth-generation~~ fifth generation European Centre Hamburg general circulation model (ECHAM5,version 5.3.02; Roeckner et al., 2003) as the atmospheric general circulation model.

2.1.1 Soil and ~~Land~~ land representation

~~The soil~~ Soil water dynamics are represented by a ~~first-generation bucket model including one layer of water storage (Delworth and Manabe~~ ~~. The soil wetness results~~ first generation bucket model with a water storage layer (Delworth and Manabe, 1988; Seneviratne et al., 2010) . Soil moisture is derived from the amount of precipitation, snowmelt, evapotranspiration, runoff, and drainage calculated by ECHAM5. ~~The interception of precipitation~~ Precipitation interception is calculated for ~~one~~ a canopy ('big leaf') layer. Surface runoff ~~originates~~ is derived from the overflow of the soil water reservoir (Delworth and Manabe, 1988; Roeckner et al., 2003). The initial state is prescribed by the geographically varying field capacity which significantly determines the model performance (Hagemann, 2002; Robock et al., 1998). The data used here were compiled from the most recent global distribution of major ecosystem types ~~made available~~ provided by the U.S. Geological Survey (Hagemann, 2002). The vegetation density (leaf area index, LAI in [~~$\mathrm{m}^2\ \mathrm{m}^{-2}$~~ $m^2\ m^{-2}$]), used to scale the leaf stomatal conductance to the canopy level, is prescribed with a ~~10-daily time-series~~ 10-day time series observed by the Ocean and Land Colour Instrument (OLCI, visible imaging push-broom radiometer) onboard the Sentinel-3 platform ~~at~~ of the Copernicus Land ~~service at~~ Service on an original grid of 1 km (Thépaut et al., 2018). This ~~represents~~ is a realistic product according to the reported LAI range of 0-6~~(Xiao et al., 2017). This data set replaces the climatology used in EMAC as standard~~ $m^2\ m^{-2}$] (Xiao et al., 2017) and replaces the standard climatology. EMAC does not include a dynamic land surface model.

2.1.2 Evapotranspiration and terrestrial photosynthesis

~~The process of evapotranspiration partially~~ Transpiration depends on the opening behaviour of the stomata (Katul et al., 2012). ~~Thus, the calculation of evapotranspiration incorporates the~~ Therefore, the stomatal conductance (g_s) is included in the calculatiobn of evapotranspiration. As already described by Schulz et al. (2001), ~~in ECHAM~~ the model formulation in ECHAM is based on the Monin-Obukov stability theory:

$$ET = -L_v \rho C_h |\mathbf{v}| \beta (q_a - h q_{sat}(T_s, p_s)) \qquad \beta = [1 + C_h |\mathbf{v}| \cdot 1/g_s]^{-1} \tag{1}$$

where L_v is the latent heat of vaporisation, ρ is the density of air~~,~~. $|\mathbf{v}|$ is the absolute value of the horizontal wind speed~~and the~~, and C_h is the transfer coefficient of heat ~~. The later two variables translate to~~ which is related by the equation: $r_a = 1/(C_h|\mathbf{v}|)$.

q_{sat} and q_a are the ~~saturation-specific~~ saturation specific and the atmospheric specific humidity~~, respectively. The relative humidity~~. h is the relative humidity at the surface ~~limits~~ by which the evapotranspiration from bare soil ~~. β determines the ratio of transpiration between~~ is limited. At $\beta = 1$ only bare soil evaporation occurs while $\beta < 1$ is used for water-stressed plants ~~(β <1) and well-watered plants (β =1)~~ (Giorgetta et al., 2013; Schulz et al., 2001). The weighted sum of the evapotranspiration over land, water and ice ~~yields~~ gives the final value per grid cell. Transpiration is ~~accounted by only a part of equation 1, namely where~~ represented by *ET* ~~is weighted by taking~~ weighted by the vegetation fraction ~~in each grid box. The stomatal~~ (per grid box, see Eq. 1). Stomatal conductance is calculated ~~by~~ using a photosynthesis scheme (A_{net}-g_s), which is based on Calvet (2000) and is ~~implemented~~ used in the IFS model (ECMWF, 2021). This approach describes the photosynthesis process and its dependence on CO_2, temperature and soil moisture (Jacobs, 1994) treating the plants as mixed crops. Currently, ECHAM/MESSy does not distinguish between different land cover types. The photosynthesis model is based on the net assimilation rate of CO_2 (~~A$_n$~~ A_n) in the plant~~varying with environmental~~. Environmental conditions (Env) and the ~~CO_2~~ CO_2 concentration outside the leaves (~~C$_s$, kg m^{-3}~~ C_s, [$kgCO_2m^{-3}$]) and inside the ~~cavities (C$_i$~~ stomata (C_i, [~~kg m^{-3}~~ $kgCO_2m^{-3}$]) ~~to yield~~ modify this process to give the stomatal conductance (~~g$_s$~~ g_s):

$$g_s = \frac{A_n(Env)}{C_s - C_i(Env)} \tag{2}$$

~~The radiation- and CO_2-limited scheme are considered for the calculation of net assimilation rate (A_n). The saturation of photosynthetic capacity A_m at high light intensities is calculated as follows:~~

$$\cancel{A_m = A_{m,max}\left[1 - \exp(-g_m(C_i - \Gamma)/A_{m,max})\right]}$$

~~with $A_{m,max}$ being the maximum photosynthetic capacity, g_m the mesophyll conductance, the compensation point at 25 °C Γ =42 ppm(for mixed crops). The two schemes are combined afterwards to yield a smooth function for A_n, which is further described in ECMWF (2021). g_m is a function of temperature and the mesophyll conductance at 25 °C where the latter involves two different factors for the water state of the atmosphere and the plant-water stress factor (for low and high vegetation) based on a non-linear, empirical expression by Calvet et al. (2004)~~Further details of the calculation are given in the supplement S1.

2.1.3 Water Stress Functions

We have investigated several water stress functions and implemented them in the stomatal conductance scheme. The dependence is ~~commonly~~ usually parameterised by a fraction of the actual soil water status limited to the availability and the plant wilting (Rogers et al., 2017). Based on the bucket model used in EMAC, the default function (*REF*) and the multiple application (described later, *DEFmulti*) ~~employs~~ uses the actual soil wetness (W_s, [m]) ~~, the critical available water (W$_{crit}$, m) and the wetness at the~~ and two thresholds according to Schulz et al. (2001):

$$f(W_s) = \begin{cases} 1 & W_s(t) \geq W_{crit}(=75\%F_c) \\ \frac{W_s(t)-W_{pwp}}{W_{crit}-W_{pwp}} & W_{pwp} < W_s(t) < W_{crit} \\ 0 & W_s(t) \leq W_{pwp}(=35\%F_c) \end{cases} \tag{3}$$

At the critical soil water level (W_{crit}, $[m]$) drought begins to reduce transpiration. The plant wilting point of plants (~~W_{pwp}, m)~~ ~~that the plant cannot extract water below this level according to Schulz et al. (2001):~~

$$f(W_s) = \begin{cases} 1 & W_s(t) \geq W_{crit}(=75\%F_c) \\ \frac{W_s(t)-W_{pwp}}{W_{crit}-W_{pwp}} & W_{pwp} < W_s(t) < W_{crit} \\ 0 & W_s(t) \leq W_{pwp}(=35\%F_c) \end{cases}$$

~~The wilting point~~ W_{pwp}, $[m]$) is the level at which plants can no go longer to extract water. It depends on soil and vegetation properties such as the soil texture and plant functional type, ~~which is however only considered indirectly by initialising~~ but is only indirectly considered by initialisation of field capacity (F_c) data and therefore introduces a ~~certain amount~~ degree of uncertainty. ~~This motivates the usage of the original plant-water~~ To overcome this uncertainty the original plant water stress formulation (*noWP*) ~~by~~ of Delworth and Manabe (1988), which considers the critical soil wetness as the ~~solely restriction for plants~~sole constraint for plants, is explored here:

$$f(W_s) = \begin{cases} 1 & W_s(t) \geq W_{crit}(=75\%F_c) \\ \frac{W_s(t)}{W_{crit}} & W_s(t) < W_{crit} \end{cases} \quad (4)$$

~~For both parametrizations~~

For both parametrisations (*REF* and *noWP*), the water stress function $f(W_s)$ is ~~considered~~ included in the calculation of the mesophyll conductance and the maximum atmospheric water deficit (in a non-linear way) (Calvet et al., 1998, 2004) which are given in section S1. Instead of ~~using a soil moisture dependent function further, we apply the plant-water stress on the~~ continuing to use a function dependent on soil moisture, we use plant water stress functions dependent on leaf water potential (ψ) according to the ~~findings~~ results of Verhoef and Egea (2014). ~~This~~ ψ is calculated according to Millar et al. (1971), ~~similarly~~ similar to the formulation ~~employed~~ used in Zhang et al. (2003):

$$\psi = -0.395 - 0.043 \cdot Temp_a \quad (5)$$

where $Temp_a$ is the air temperature (in [°C]). The stress factor (*LWPfrac*) is calculated (similarly to Eq. 3) according to Zhang et al. (2003):

$$f(\psi) = \begin{cases} 1 & \psi \geq \psi_{io} \\ \frac{\psi - \psi_{crit}}{\psi_{io} - \psi_{crit}} & \psi_{io} > \psi > \psi_{crit} \\ 0 & \psi \leq \psi_{crit} \end{cases} \quad (6)$$

where $\psi_{io} = -0.74$ MPa is the leaf water potential at initial reduction, and $\psi_{crit} = -2.75$ MPa the leaf water potential at final stomatal closure (Verhoef and Egea, 2014).

However, by evaluating the ~~several~~ different stomatal models, Sabot et al. (2022) shows that an exponential ~~dependency~~ dependence of ψ is more ~~suitable~~ appropriate (*LWPexp*):

$$f(\psi) = \begin{cases} 1 & \psi \geq 0 \\ e^{s_{Med} \cdot \psi} & \end{cases} \tag{7}$$

where $s_{Med} = 2\ MPa^{-1}$ is a sensitivity parameter. We ~~further~~ have also implemented the more sophisticated stress factor used in the common Community Land Model (CLM5, (Kennedy et al., 2019)) as reference (*CLM5*):

$$f(\psi) = \begin{cases} 1 & \psi \geq 0 \\ 2^{-(\frac{\psi}{p50})^{c_k}} & \end{cases} \tag{8}$$

where the water potential at 50 ~~%~~ % loss of stomatal conductance ($p50 = -1.75$, in [MPa]) and a vulnerability parameter ($c_k = 2.95$) are ~~used. Please note~~ included. Note that in CLM5 this function uses the soil matric potential ~~is used~~instead. However, the leaf water potential can be ~~used~~ considered as a proxy (Kozlowski et al., 1991; Verhoef and Egea, 2014).

A quantitative ~~limitation~~ constraint analysis by Egea et al. (2011) found that for a realistic model representation water stress should ~~act at least on~~ at least affect the biochemical capacity and stomatal conductance and alternatively also on the mesophyll conductance. ~~In~~ However, most ecosystem models, ~~however, only~~ only include biochemical or stomatal limitations~~are included. Therefore, we apply the plant-water stress in case~~ . For *DEFmulti*, *LWPfrac*, *LWPexp* and *CLM5*, we apply plant water stress linearly to the stomatal and the mesophyll conductance ~~as well as~~ and to the photosynthetic activity of plants.

An overview of all ~~parametrizations~~ parametrisations used as plant-water stress factor in the calculation of stomatal conductance is given in Table 1.

2.2 ~~Observational data~~

2.1.1 ~~EUMETSATThe observational data for evapotranspiration was generated~~ Experimental design

We perform dynamical simulations with 3-hourly instantaneous and average output for each plant water stress parametrisation at mesoscale (T106: 1.12 ° or ≈ 60km, middle atmosphere) for the period 2017/2018. The dynamical simulations apply a set of submodules (AEROPT, CLOUD, CLOUDOPT, CONVECT, GWAVE, MSBM, OROGW, ORBIT, QBO, RAD, SURFACE, TROPOP, VERTEX), similar to the set up used in Jöckel et al. (2016). The land–atmosphere exchange and vertical diffusion in EMAC is described here by the submodel VERTEX (Emmerichs et al., 2021). The main functionalities of VERTEX are explained in section 2.1.2. The warm spell metric is calculated from a dynamical simulation at T42 (2.79 ° or ≈ 300km) covering the period 1979-2008. To assess the impact on air pollution (see Sect. 3.5), we perform two chemical simulations (T106, 2017/2018). These simulations additionally use submodules describing emissions of atmospheric species (OFFEMIS, ONEMIS, BIOBURN, LNOX), gas exchange submodels (DDEP, AIRSEA) and chemistry submodules (MECCA, JVAL).

Case	Plant-water stress factor	**current study** (original study)
noWP	$f(W_s) = \begin{cases} 1 & W_s(t) \geq W_{crit}(=75\%F_c) \\ \frac{W_s(t)}{W_{crit}} & W_s(t) < W_{crit} \end{cases}$ (1)	applied in g_m calculation (to final g_s)
REF	$f(W_s) = \begin{cases} 1 & W_s(t) \geq W_{crit}(=75\%F_c) \\ \frac{W_s - W_{pwp}}{W_{crit} - W_{pwp}} & W_{pwp} < W_s < W_{crit} \\ 0 & W_s(t) \leq W_{pwp}(=35\%F_c) \end{cases}$ (2)	applied in g_m calculation (to final g_s)
DEFmulti	as *REF* (1,3)	multiplicative factor to g_m, g_s, A_{max}
LWPfrac	$f(\psi) = \begin{cases} 1 & \psi \geq \psi_{io} \\ \frac{\psi - \psi_{crit}}{\psi_{io} - \psi_{crit}} & \psi_{io} > \psi > \psi_{crit} \\ 0 & \psi \leq \psi_{crit} \end{cases}$ (4)	multiplicative factor to g_m, g_s, A_{max} (to g_s)
LWPexp	$f(\psi) = \begin{cases} 1 & \psi \geq 0 \\ e^{s_{Med} \cdot \psi} & \end{cases}$ (5)	multiplicative factor to g_m, g_s, A_{max} (to the slope of the sensitivity of g_s to A_n)
CLM5	$f(\psi) = \begin{cases} 1 & \psi \geq 0 \\ 2^{(-\frac{\psi}{p50})^{c_k}} & \end{cases}$ (6)	multiplicative factor to g_m, g_s, A_{max}

Table 1. Parametrisations for plant-water stress used here, originally by Schulz et al. (2001) (1), Delworth and Manabe (1988) (2), Verhoef and Egea (2014) (3), Zhang et al. (2003) (4), Sabot et al. (2022) (5), CLM5,Kennedy et al. (2019) (6) with g_m, g_s, A_{max} being the mesophyll conductance,and stomatal conductance, the maximum photosynthetic capacity. W_s, W_{crit},W_{pwp} are the actual soil wetness, critical soil wetness and soil wetness at wilting point, respectively. F_c is the field capacity (maximum holding capacity of soil moisture). ψ, ψ_{crit} and ψ_{io} are the actual leaf water potential, the critical value, the value at final stomatal closure, respectively. c_k, $p50$ and s_{med} are a vulnerability parameter, water loss at 50 $\%$ stomatal closure and sensitivity parameter, respectively.

The chemical mechanism includes the basic gas phase chemistry of ozone, methane, and odd nitrogen with in total 310 reactions and 155 species as in Jöckel et al. (2016). The dry deposition of trace gases on vegetation is calculated according to the multiple resistance scheme, which uses the stomatal resistance calculated in VERTEX. The scheme is used here with six generalised land types. The vegetation canopy is represented as a single system; i.e. the detailed structure and plant characteristics are neglected (one big leaf approach). The leaves are oriented horizontally and the leaf density is uniformly distributed vertically (Kerkweg et al., 2006; Emmerichs et al., 2021). Further information regarding the submodules can be found in Jöckel et al. (2010, 2016). Two additional chemistry simulations comprise the CO_2-doubling experiments.

To reproduce the large-scale model dynamics, (i.e the jet stream) the horizontal winds (divergence, vorticity) are nudged towards reanalysis data of the ERA5 reanalysis data by Newtonian relaxation as it is applied as selective nudging to perform storyline simulations (Shepherd et al., 2018). This allows the model thermodynamics to respond freely to the process modifications implemented in this study.

2.2 Observational data

2.2.1 EUMETSAT

Evapotranspiration observations have been provided by the European Organisation for the Exploitation of Meteorological ~~Satellite~~ Satellites (EUMETSAT) ~~with~~ using the second generation of geostationary Meteosat satellites~~which cover the domain~~. This covers the area of Europe, Africa and most of South America ~~at~~ with a spatial resolution of 3 ~~km spatial resolution~~ km. The Spinning Enhanced Visible and Infrared Imager (SEVIRI) radiometer operating (among others) on board ~~obtains the radiation components at the surface . This datatogether with further~~ provides the surface radiation component. These data, other biophysical parameters and soil moisture data from remote sensing, recent ~~land-cover~~ land cover information from the ECOCLIMAP land cover database and meteorological fields from numerical weather prediction drive a physical model of the energy exchange between the soil-vegetation-atmosphere ~~systems~~system. By this, the flux [in ~~$mm\ h^{-1}$~~$mm\ h^{-1}$] of water evaporated at the ~~Earth-atmosphere~~ earth-atmosphere interface (soil, vegetation, water bodies) and transpired by vegetation through stomata (as a consequence of photosynthetic processes) is calculated within a ~~Soil-Vegetation-Atmosphere~~ soil-vegetation-atmosphere Transport model (SVAT) (saf, 2018):

$$ET = 3600\frac{LH_T}{L_v}, \qquad LH_T = \frac{L_v\rho}{(r_a+r_s)}[q_{sat}(Temp_s)-q_a(Temp_a)] \tag{9}$$

where LH_T is the latent heat flux of transpiration in $[W/m^2]$, L_v the latent heat of water ~~vapor~~ vapour in [~~J kg^{-1}~~ $J\ kg^{-1}$], ρ the air density [~~kg m^3~~$kg\ m^3$], r_a and r_s are the aerodynamic and stomatal resistances (inverse of the ~~conductances~~conductance), q the specific humidity and $q_{sat}(T_s)-q_a(T_a)$ the atmospheric saturation deficit in [~~kg/kg~~kg/kg]. ~~This product~~ These products have been downloaded from the website of the EUMETSAT ~~land surface analysis~~ Land Surface Analysis (LSA SAF) ~~consortium~~ Consortium website (https://landsaf.ipma.pt/ChangeSystemProdLong.do?system=LandSAF+MSG&algo=DMET, last ~~access~~accessed: 29.06.2023) ~~at~~ with a time interval of 3 hours (original frequency: 30 min). For comparison with the model results, the downloaded dataset was regridded to the ~~spatial grid of EMAC~~EMAC spatial grid. The product validation report found a general accuracy of 20-25 ~~%,~~ %, which is equivalent to the accuracy of measurements. ~~Main uncertainties may stem from~~ The main uncertainties may be due to the physical formalism of the algorithm, the errors of the input data errors, surface heterogeneity and sensor performance among others (saf, 2018).

2.2.2 GLEAM

The Global Land surface Evaporation: the Amsterdam Methodology (GLEAM) model estimates the evaporative flux over land by assimilating satellite observations. ~~The land~~ Land evapotranspiration is the sum of the bare soil, short vegetation, and tall vegetation in each grid box. The soil water content of ~~multiple~~ several layers (depending of the land type) is calculated by a water balance between the input snowmelt and rainfall (minus interception). ~~Thereby, surface~~ Surface soil moisture observations from satellites are assimilated (~~with~~ using the Kalman filter approach) at a daily time step based on ~~its~~ their uncertainty. The Priestly-Taylor equation calculates the potential latent heat flux λE_p $[MJm^{-2}]$:

$$\lambda E_p = \alpha \frac{\Delta}{\Delta + \gamma}(R_n - G) \tag{10}$$

as a function of the net radiation (R_n, daily ~~observational data~~observations) and the ~~ground-heat~~ ground heat flux (G). Δ is the slope of the temperature/saturated ~~vapor~~ vapour pressure curve (in $[k\ Pa\ K^{-1}]$). ~~The division~~ Division by the latent heat of vaporisation λ ~~yields~~ gives the potential evaporation (E_p in [~~mm~~mm]). For optimal environmental conditions, $\alpha = 0.8$ and $\alpha = 1.26$ ~~at~~ are used for tall and short vegetation (or bare soil)~~are used~~, respectively. An evaporative stress (S) is used to convert E_p to actual transpiration (T in ~~$[mmday^{-1}]$~~$[mm\ day^{-1}]$, over vegetation):

$$T = SE_p \tag{11}$$

S is parameterised separately for tall and short ~~canopies as well as~~ canopy and for bare soil (then eq. 11 yields bare soil evaporation) based on the observed soil moisture conditions and ~~vegetation optical depth . The canopy~~ optical depth of vegetation. Canopy interception loss (I) is estimated in a separate module based on observations of daily ~~rainfall~~precipitation, snow depth, tall canopy fraction and lightning climatology and parameters for canopy cover, canopy storage, mean ~~rainfall~~ precipitation and evaporation rate ~~during~~ under saturated canopy conditions. ~~To account for conditions with wet canopy where water is evaporated (and not intercepted) the factor $\beta = 0.07$ is introduced. An extra~~ The use of an interception loss fraction (β =0.007) ensures that wet canopy evaporation is only considered once in the calculation. An additional module estimates the snow and ice sublimation for the snow-covered pixels (no stress) where α =0.95. ~~The evaporation~~ Evaporation from lakes and rivers is not included. ~~Further~~ More details can be found in Miralles et al. (2011). The data ~~was~~ have been downloaded from the ftp server after registration https://www.gleam.eu/#downloads, last access: 24.07.2023).

2.2.3 TROPOSIF

~~Solar-induced~~ Solar induced chlorophyll fluorescence (SIF) ~~,~~ can be observed using remote sensing. This is an electromagnetic signal emitted by the chlorophyll of assimilating plants ~~and~~ that is not used for photosynthesis~~, can be observed with remote sensing~~. This can be a proxy for photosynthetic activity~~because~~ , as the SIF signal ~~responds to perturbations~~ is sensitive to perturbations caused by environmental stress (Maes et al., 2020). However, the estimation requires high spectral resolution and advanced retrieval schemes since the emissions contribute only a small fraction ~~to~~ of the radiance. The TROPOMI (TROPOspheric Monitoring Instrument) instrument ~~aboard~~ on board the Copernicus Sentinel-5 Precursor mission, launched in October 2017, measures ~~Top-of-the-Atmosphere radiances. By inversion of a linear forward model these~~ top-of-the-Atmosphere radiances. These are fitted in the far-red spectral region by inverting a linear forward model. SIF estimates from the 743-758 nm window are the most robust ~~against atmospheric effects like~~ to atmospheric effects such as cloud contamination. The L2B product used here (SIF dataset from TROPOMI: TROPOSIF) combines all observations at the ~~single orbits within one~~ individual orbits into an ungridded netCDF4 file (NOVELTI et al., 2021). The evaluation with other SIF products showed a general consistency in terms of level and amplitude of the retrieved SIF, and seasonality, for vegetated surfaces. The indicative error threshold for the definition of spatio-temporal bins is 0.2 ~~mW m^{-2} steradian^{-1} nm^{-1}~~

$mW\ m^{-2}\ steradian^{-1}\ nm^{-1}$ value (about 10 ~~% of the~~ % of the globally observed peak SIF values~~observed globally~~) (Guanter et al., 2015). This ~~translate~~ corresponds to 0.064 ~~mm day^{-1}~~ $mm\ day^{-1}$ of transpiration. In addition, the data product includes a quality flag which is used here for individual quality assurance. The data can be downloaded ~~at~~ from http://ftp.sron.nl/open-access-data-2/TROPOMI/tropomi/sif/v2.1/l2b/ (NOVELTI et al., 2021; Guanter et al., 2015). According to Maes et al. (2020) ~~the~~ SIF ~~data~~ can be converted to the latent heat flux of transpiration (LH_T in $[W/m2]$):

$$LH_T = 61.4 \cdot SIF \tag{12}$$

Using the latent heat of water ~~vapor~~ vapour ($L_v = 1.5 \cdot 10^6$ in [~~J kg^{-1}~~ $J\ kg^{-1}$]) gives the transpiration [~~mm day^{-1}~~$mm\ day^{-1}$]:

$$T = LH_T / L_v \cdot 3600 \tag{13}$$

To compare this dataset to the EMAC model we sample the instantaneous output along the satellite orbit at 13:30 UTC.

Estimation method	**Plant transpiration**	**Evapotranspiration**
EMAC	considers β only for the vegetation fraction	$ET = -L_v \rho C_h \lvert\mathbf{v}\rvert \beta(q_a - hq_s(Temp_s, p_s))$ $\beta = [1 + C_h \lvert\mathbf{v}\rvert R_{stom}]^{-1}$
Satellite observations by EUMETSAT	not provided	$ET = 3600 \frac{LE}{Lv}$ $LE = \frac{L_v \rho}{(r_a + r_s)}[q_{sat}(Temp_s) - q_a(Temp_a)]$
GLEAM model driven by satellite observations	$T = SE_p$	$ET = T + I - \beta I$
Estimate from solar-induced fluorescence by TROPOMI	$LH_T = 61.4 \cdot SIF$ $T = LH_T / L_v \cdot 3600$	not provided

Table 2. Formulae for plant transpiration and evapotranspiration from EMAC and the used observational datasets.

3 Results and Discussion

3.1 Plant-water stress and transpiration

The stress functions ~~summarized~~ summarised in Table 1 ~~yield~~ result in a variety of different ~~plant-water stress~~ plant water stresses and thus transpiration. Figure 1 ~~provides~~ gives a first overview of how the response functions vary with proxies ~~of~~ for water stress (soil moisture and leaf water potential). ~~Lowering~~ Decreasing 'volumetric' soil moisture (soil wetness divided by the field capacity) linearly increases ~~the plant-water~~ plant water stress for the ~~cases~~ *REF* and *DEFmulti* cases (black line) until the wilting point (35 ~~%~~ % of the field capacity) is reached. ~~With~~ By using the *noWP* function (~~gray~~ grey line), ~~contrarily,~~ plants experience a ~~weaker stress with drying soil , which, however, can increase up~~ lower level of stress as the soil dries, but

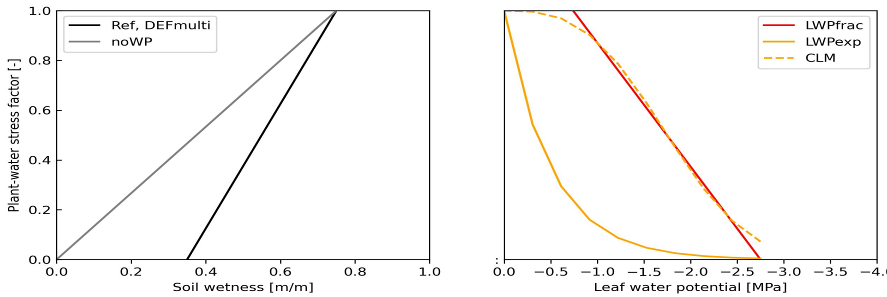

Figure 1. Plant-water stress factor vs. (volumetric) soil wetness (left) and leaf water potential (right) of described ~~parametrizations~~parametrisations.

this can increase to the point of stomatal closure (stress factor= 0). The ~~functions~~ *LWPfrac* and *CLM5* ~~show mostly~~ functions mostly show a linear increase ~~of~~ in the stress with increasing water demand (more negative ψ). The *CLM5* function ~~covers also~~ also covers the ψ range between 0 and -1 [MPa] where the response is much weaker. *LWPexp* is a simple exponential function with a steep increase ~~of~~ in the stress response for ψ ~~from~~ between 0 and -1 [MPa]. In comparison, for most plant species Verhoef and Egea (2014) observed a sigmoidal ~~dependency of~~ dependence for most plant water stress on soil water (their Figure 1). The recent modelling study by Harper et al. (2021) ~~applied~~ used a function with a simple quotient depending on soil moisture similar to the functions *REF* and *DEFmulti*. ~~Model improvements were obtained by replacing the~~ They obtained model improvements by replacing soil moisture with the soil matric potential~~(Harper et al., 2021)~~, for which ψ ~~applied~~ (used in *LWPfrac*) can be used as a proxy (Kozlowski et al., 1991; Verhoef and Egea, 2014). Early observations of increasing stomatal conductance with ~~a increase of~~ increasing ψ (to lower negative values, see Figure 2B in Sellers et al. (1997)) are ~~in general agreement~~ generally consistent with these results.

~~We explore the changes on global and regional scales using spatial (weighted) means for different regions: Europe (oceanic), South America Monsoon (tropical monsoon), Arabian Peninsula (hot arid), African Savanna, boreal forest (continental), East Asia (warm temperate moist). The sensitivity analysis of *noWP* and *DEFmulti* simulations shows only small local changes in transpiration (within the monthly range of variance), impacting the annual estimate only by ±10-15 %. This is because neglecting the wilting point decreases the plant-water stress (~~f_{W_s}~~) by only 10 % in all dry vegetated regions (dry climate:~~ ~~$W_s < 0.35 * F_c$~~~~, see Seneviratne et al. (2010)) and thus transpiration is only marginally affected.~~

Figure 2 shows the simulated annual mean maximum photosyntetic capacity ($A_{m,max}$) and transpiration (T) and ~~the respective~~ their changes. The global distribution (simulated by *REF*) follows the spatial distribution of air temperature and CO_2 concentration in the leaf ~~cavities~~stomata. $A_{m,max}$ is strongly driven by leaf (2m) temperature, as shown in Fig. 2a. Until the ~~up-sealing~~ upscaling of stomatal conductance to the canopy level (see ECMWF (2021), eq. 8.123) the intermediate calculations, e.g. for $A_{m,max}$, are at the leaf level. Thus, the distributions over non-vegetated areas ~~like the Saharian~~ such as the Sahara desert are masked out here (vegetation fraction>1%) which depends on the model vegetation mask. Transpiration (Figure 2b) ~~additionally~~ also depends on atmospheric moisture, which explains its maxima in ~~the~~ tropical rainforests. The multiple application of the default stress factor (to g_m, $A_{m,max}$, g_s: *DEFmulti*) leads to small decreases of $A_{m,max}$ (Figure 2c) in dry areas (SM< W_{pwp}, ~~soil-moisture~~ soil moisture limited). Thus, transpiration is not significantly ~~changed~~ altered (Figure 2d, max=0.5).

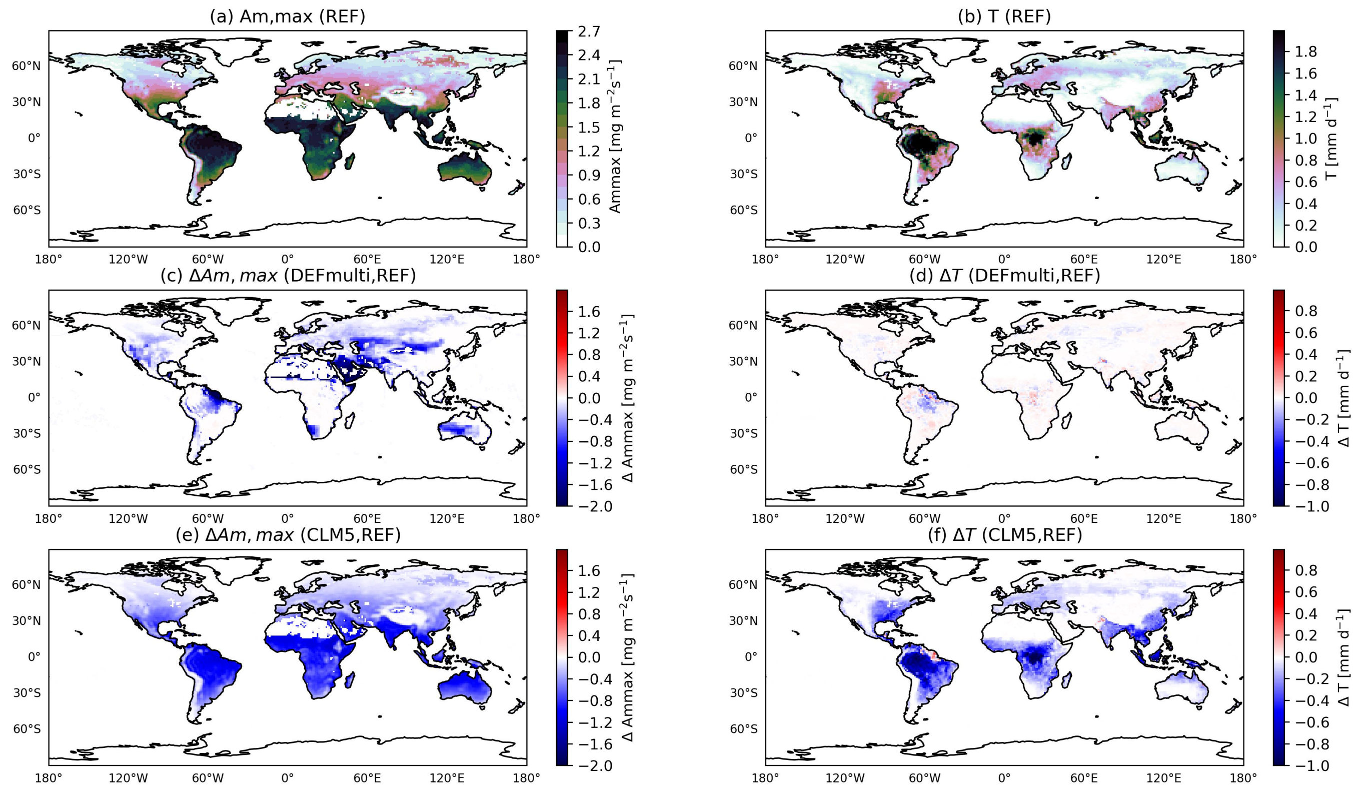

Figure 2. Annual mean maximum CO_2 assimilation rate ($A_{m,max}$) (a), transpiration (T) (b) and the respective changes to *DEFmulti* (c,d) and *CLM5* (e,f), mask for vegetated region (vegetation fraction>1%).

The ~~impact of the plant-water~~ effects of the plant water stress functions based on ~~leaf-water~~ leaf water potential (e.g. *LWPfrac*) ~~is~~ are more widespread in vegetated areas ~~since the parametrization~~ as the parametrisation is temperature driven. $A_{m,max}$ (equation S2) and also the daily transpiration decreases significantly by 1-2 ~~mm day^{-1}~~ $mm\ day^{-1}$ which is highest in the tropical rainforest (Figure 2f). This can be ~~reasoned~~ explained by the radiation maximum in the inner tropics~~which leads to a higher influence of~~ . Therefore, the 30 ~~% increase of the plant-water stressand subsequent decrease of the~~ % increase in plant water stress, the subsequent decrease in maximum photosynthetic capacity ~~(Figure 2e)~~ and mesophyll conductance (not shown here) has a greater influence in the tropics compared to ~~SH continents~~other regions on the SH continents (Figure 2e). With the ~~start~~ onset of the boreal summer in May/June~~the impact~~ , the influence spreads out to Europe and the ~~US~~ USA, while it's limited to the evergreen tropical forests on the SH. ~~Note, that also the final stomatal conductance is lowered again by the stress factor. The changes of~~ The changes in the sensitivity simulations *LWPexp* and *CLM5* (not shown here) have the same spatial distribution~~only a minor different change of the plant-water stress and subsequent variables among each other which means that the linear fraction and the exponential formulation~~. In the regional plots (Fig. 3), there is only a small difference between the changes in plant water stress and the subsequent variables. Thus, the linear and exponential formulations can be interpreted ~~similarly~~in a similar way. All three stress functions based on leaf water potential *LWPfrac*, *LWPexp*, *CLM5*) introduce an additional dependence of the modelled transpiration ~~to~~ on air temperature (except in the arid climate). In fact, this slows down the increase ~~of transpiration with rising~~ in transpiration with increasing temperature. Accordingly, the amplitude of the diurnal cycles decreases (Figure 3~~when introducing the multiple stress factor application (*LWPfrac*, *LWPexp*, *CLM5*~~). On the other hand, the ~~cycle of plant-water stress show firstly variationsduring day~~ diurnal cycle of plant water stress initially shows variations, which is an observed ~~phenomena~~ phenomenon according to Xiao et al. (2021). In contrast to *LWPfrac* and *CLM5*, which predict not only the same ψ but also the same $f(\psi)$, *LWPexp* estimates a higher (negative) ψ in most regions (shown in Figure 3). This can be explained ~~via~~ by the temperature-transpiration feedback expected in ~~dry~~ arid climates (ARP and African ~~savanna~~savannah). In addition, the simple exponential function in *LWPexp* ~~yields~~ gives a stress factor close to zero and thus unrealistically shuts down the mesophyll conductance and the photosynthetic activity~~in contrast to~~, unlike *LWPfrac* and *CLM5*. Analysis of the *noWP* and *DEFmulti* simulations shows only small local changes in transpiration (within the monthly variance range) affecting the annual estimate by only ±10-15 %. This is because neglecting the wilting point reduces plant water stress (f_{W_s}) by only 10 % in all dry vegetation regions (dry climate: $W_s < 0.35F_c$, see Seneviratne et al. (2010)) and thus transpiration is only marginally affected.

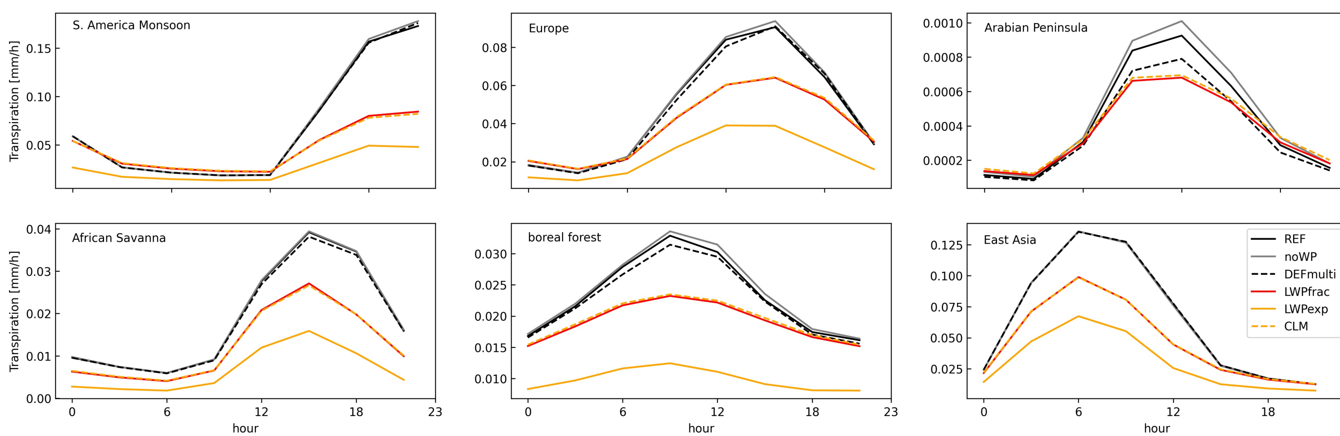

Figure 3. Regional mean diurnal cycle of transpiration in South America Monsoon region, Europe, Arabian peninsula, African Savanna, boreal forest and East Asia in boreal summer. The regions are defined in the respective order with the following scientific regions: 12; 16-18; 36, 21; 18,29,30,31,2,1; 35) according to the IPCC reference definitions (Iturbide et al., 2020).

3.2 Global estimates of transpiration

All EMAC simulations show a realistic spatial variation of annual transpiration (Figure 2b). However, the low global VR values globally (Table 3) indicate that the simulated variability is lower (VR<1) compared to the GLEAM dataset. This cannot be attributed to an oversimplification of the modelled process~~because~~. GLEAM is based on the Priestley-Taylor equation, an empirical equation dependent on solar radiation and temperature, compared to the ~~physical-based~~ physically based Penman-Monteith approach used in EMAC (Table 2~~. The reference simulation of EMAC~~). The EMAC reference simulation with the standard ~~plant-water~~ plant water stress overestimates the global ~~average~~ mean transpiration calculated with GLEAM by 46 ~~mm yr^{-1}~~ $mm\ yr^{-1}$ (16 ~~%~~%, Table 3), which is well within the uncertainty range of the GLEAM product ($\pm$ 136 ~~mm yr^{-1}~~$mm\ yr^{-1}$). The *LWPfrac* and *CLM5* stress factors correct ~~for~~ this overestimation regionally. The ~~global average, however, the new~~ new global (mean) model estimate of 276/277 ~~mm yr^{-1}~~ $mm\ yr^{-1}$ is lower than the GLEAM estimate. Compared to the GLEAM uncertainty, all model simulations show a higher 1 σ (standard deviation) range, indicating a higher uncertainty~~which e.g. couldbe attributed~~, which could, for example, be due to the representation of precipitation in the model. In GLEAM, ~~instead, precipitation stems~~ however, precipitation is derived from satellite observations (~~s.~~ see section 2.2.2). A lower 1σ in the sensitivity simulations based on the leaf water potential ~~indicate~~ indicates an improvement due to ~~neglecting~~ the neglect of the uncertain soil moisture data usually used in the model. ~~Utilising~~ The use of the transpiration estimate from the TROPOSIF data ~~yields~~ gives a good comparison with the (monthly mean) model predictions (only ~~low~~ small underestimation) over areas with high transpiration (e.g. Europe, East Asia) in spring and late autumn. Under strong drought conditions, ~~solar induced~~ solar-induced plant fluorescence by plants decouples from transpiration (Maes et al., 2020) and thus the linear relationship between *SIF* and *T* (applied here) is ~~not validanymore~~ no longer valid, e.g. during the boreal summer (Martini et al., 2022). ~~Compared~~ However, compared to GLEAM (masked for the TROPOSIF region)~~however~~, the TROPOSIF dataset predicts ~~a~~ lower daily transpiration ~~during~~ in spring and higher transpiration ~~during~~ in autumn. The seasonality of SIF strongly follows the growing season on the NH~~which might induce some mismatches~~, which may cause some discrepancies.

Datasets	**Transpiration (1σ)** [~~mm yr^{-1}~~$mm\ yr^{-1}$]	**NAE**	**VR**
GLEAM	329.1 ($\pm$ 68)	-	-
REF	375.7 ($\pm$ 98)	5.00	0.08
noWP	379.6 ($\pm$ 100)	5.59	0.07
DEFmulti	370.1 ($\pm$ 97)	9.80	0.08
LWPfrac	277.2 ($\pm$ 77)	4.85	0.11
LWPexp	166.9 ($\pm$ 45)	10.57	0.22
CLM	276.2 ($\pm$ 76)	4.89	0.11

Table 3. The global estimates of transpiration (1σ - standard deviation), normalised absolute error (NAE) and the variance ratio (VR: $\frac{var(mod)}{var(obs)}$, accounting for grid boxes with more than 1 ~~%~~ % vegetation.

~~The~~ Taking into account the multi-model *ET* estimate ~~of~~ from 18 CMIP6 models (1980-2014, ~~general increase of ET~~ ET grows with time) and the observation-based T/ET ratio of 64 % ~~by Pan et al. (2020)yield a~~ from Pan et al. (2020), an estimated global transpiration of 384 ~~mm yr^{-1}. From this, it~~ $mm\ yr^{-1}$ is obtained. It can be concluded that all model estimates in our study predicted annual transpiration reasonably well. The only exception is the sensitivity simulation *LWPexp*~~showing an unrealistic strong reduction~~ , which shows an unrealistic large reduction and thus a high normalised absolute bias (NAE)~~which is likely~~ , probably due to the choice of ~~parameters constraining the stress factor significantly (s.~~constraining parameters (see 7). For the further impact assessment in this study, we use the stress factor *LWPfrac*~~since it overall shows the best performance~~ , as it performs best overall (slightly better than the *CLM5* factor).

3.3 Contribution to ~~global evapotranspiration~~Global Evapotranspiration

The contribution of transpiration to the total *ET* varies in time and space with vegetation and soil characteristics (Wang and Dickinson, 2012; Cao et al., 2022; Lian et al., 2018). This spatial variability is reflected ~~by~~ in GLEAM and EMAC~~whereas especially the estimates~~ , where the estimates are particularly inconsistent in Europe and Africa ~~mismatch~~ (Figure 4). ~~The~~ Lian et al. (2018) reports a dominance of soil evaporation over transpiration in ~~dry~~ arid (non-vegetated) regions~~as reported by Lian et al. (2018)~~ . This is here also shown ~~in the African~~ here in the Sahara desert by a low T/ET ratio (in GLEAM and EMAC) and in non-vegetated parts of China (EMAC). ~~Also~~Similarly, the low T/ET ratio in ~~northernmost areas~~ the northernmost (partly snow-covered) areas of Canada and Siberia (~~see~~ as shown in Lian et al. (2018)) is only captured by EMAC (not by GLEAM). In humid regions, especially in the tropics, evapotranspiration is driven by transpiration. The contribution can ~~reach~~ be up to 87 ~~%~~ % over densely vegetated regions. ~~For comparison, observations in the Amazonian~~ Observations in the Amazon tropical forest indicate an average T/ET ratio of 0.7 (Wang and Dickinson, 2012; Zhang et al., 2017). This can be consistently represented by EMAC (Figure 4b) although the sensitivity simulations, e.g. *LWPfrac* and *CLM5*, partly reduce the T/ET ratio too much in the ~~south of the South America continent~~ southern Argentina (Figure 4c,d). According to the simulated and ~~observation-based~~ observational estimates of T/ET by Lian et al. (2018) (their Figure 1a), all EMAC simulations represent too low values in most parts of U.S., suggesting a dry model bias. For the central U.S., Dong et al. (2022) indeed confirms that unbiased estimates of summertime daily maximum temperature ~~could be achieved only~~ can only be achieved with a T/ET ratio of 0.7. ~~Contrarily~~In contrast, GLEAM shows higher values of the T/ET ratio for the east coast of the ~~U.S~~USA. as well as for the SH continents, Europe, and Asia. ~~The incorrect~~ Incorrect E-T partitioning ~~was identified as an error source of~~ has been identified as a source of error in ET estimation in CMIP5 models (Lian et al., 2018).

To assess the model estimation of evapotranspiration we compare with *ET* estimates ~~by~~ from GLEAM and EUMETSAT~~whereas GLEAM shows generally~~ . GLEAM generally gives higher estimates (Figure 5a, c). *ET* has its maximum in the tropics while in the high northern latitudes and sparse-vegetated areas (e.g. ~~South African~~ Sahara desert) low values occur. The GLEAM estimate ~~of~~ (EUMETSAT-region) of *ET* (512 mm ~~yr^{-1}~~yr^{-1}) differs by 30 ~~mm yr^{-1}~~ $mm\ yr^{-1}$ (6 ~~%~~%) from the EUMETSAT value (481 ~~mm yr^{-1}~~$mm\ yr^{-1}$) which could be considered to be within the uncertainty range. However, regionally the difference can be large, as much as 50 %. This is most evident in the tropics and consistent with recent studies~~reporting a large spread and a high uncertainty in model estimates for *ET* at low latitudes due to the parametrization of the root water~~

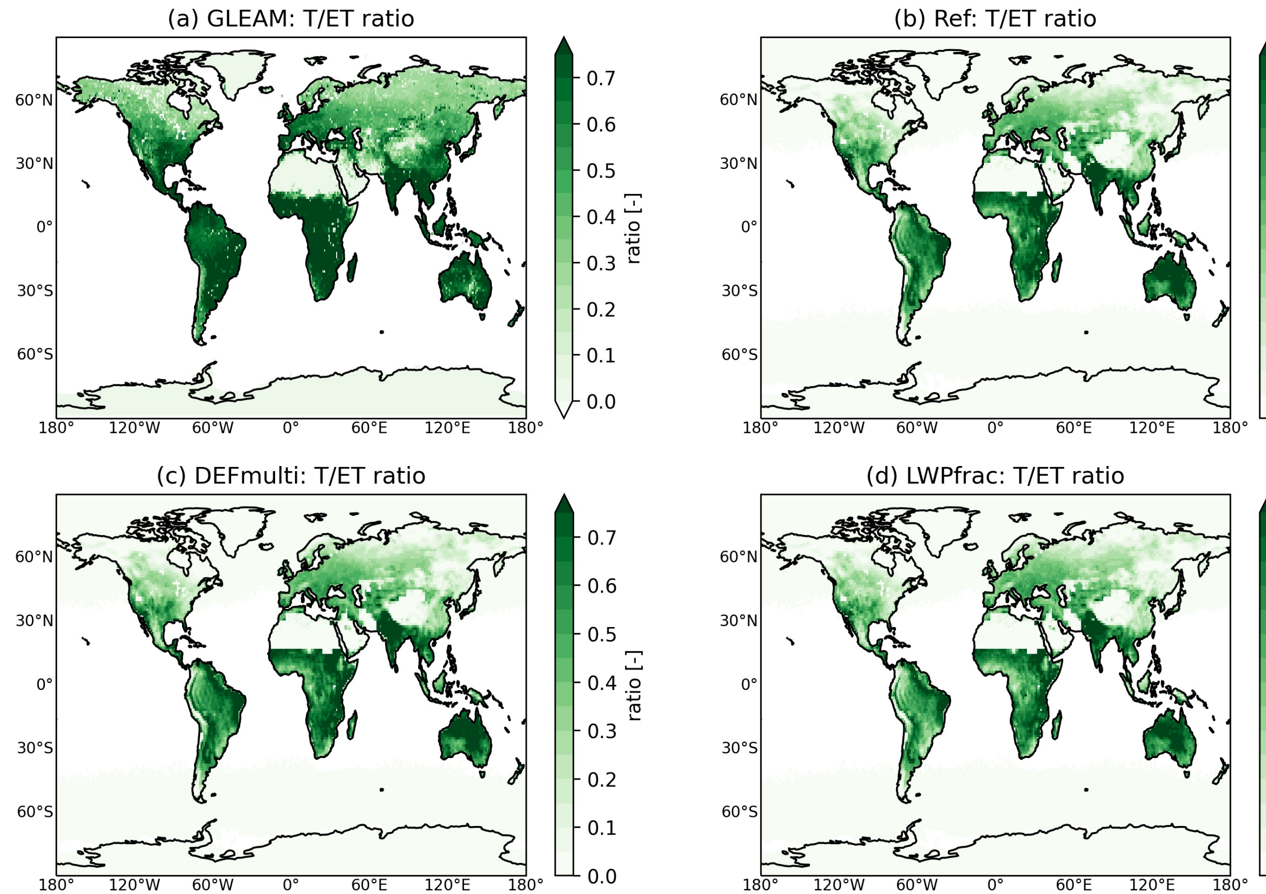

Figure 4. Annual mean ratio of transpiration evapotranspiration by (a) GLEAM, (b) *REF*, (c) *DEFmulti*, and (d) *LWPfrac* ~~).~~ in 2018.

~~uptake (Pan et al., 2020). According~~ . Compared to literature values by ~~(e.g., Elnashar et al., 2021)~~(Elnashar et al., 2021), who calculated an annual *ET* of 540 ~~mm yr^{-1}~~ $mm\ yr^{-1}$ (for 2018), the GLEAM estimate is the most consistent~~with literature values~~. Thereby, the models usually differ by 200 ~~mm yr^{-1}~~ $mm\ yr^{-1}$ which is about twice the spread of estimates by single models (minima and maxima) (Wang et al., 2021). In a model intercomparison Pan et al. (2020) report a large spread and a high uncertainty in model estimates for *ET* at low latitudes due to the parametrisation of the root water uptake.

The global average of annual *ET* predicted by EMAC with the different ~~plant-water stress parametrizations~~ plant water stress parameterisations is about 425-480 ~~mm yr^{-1}.~~ $mm\ yr^{-1}$. The ET predicted by the *CLM5* sensitivity simulation, which ~~reproduces transpiration the best (see Sec. 3.2, together with *LWPfrac*) ,~~ best reproduces transpiration (see section 3.2) compares well with the GLEAM annual values. ~~Mainly~~ Especially, in some coastal areas~~like East~~ , such as the eastern U.S. ~~, NE Amazonconsiderable differencesoccur~~ and the northeastern Amazon, there are significant differences, which could be ~~reasoned by~~ due to neglected sub-scale ~~hydrology at the coasts~~ coastal hydrology (Figure 5b). Compared to EUMETSAT, EMAC (as

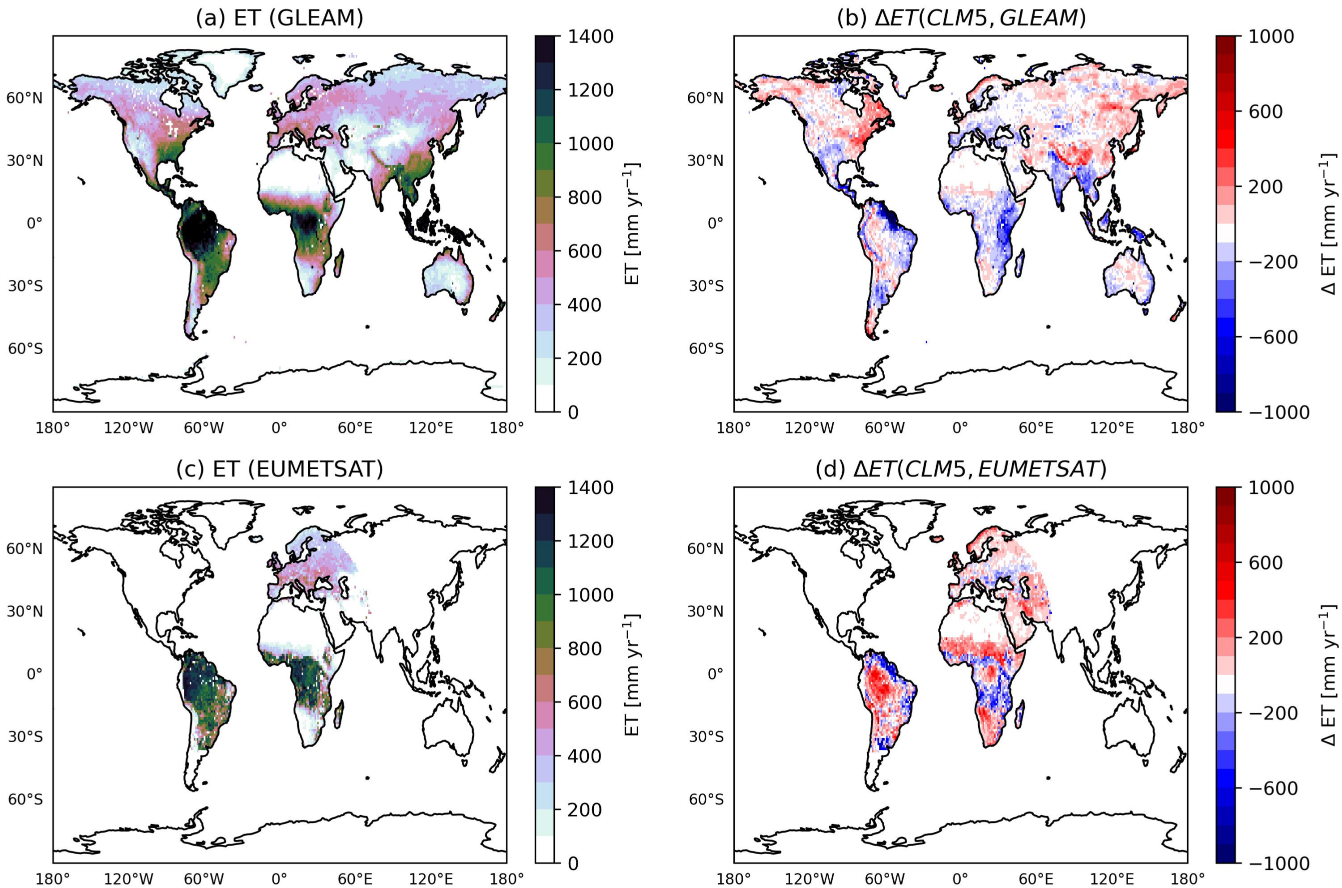

Figure 5. Annual mean evapotranspiration (*ET*) of (a) GLEAM, and its difference to (b) the *CLM5* sensitivity simulation (*CLM5*-GLEAM), (c) annual evapotranspiration (*ET*) of EUMETSAT and (d) the difference to the ~~the~~ *CLM5* sensitivity simulation.

well as GLEAM) estimates a higher annual mean *ET* in tropical ~~rain forests whereas~~ rainforests, while in tropical monsoon climate ~~region~~ regions it simulates too low values ~~are simulated~~ compared to EUMETSAT (Figure 5d). This pattern of differences ~~suggests precipitation as a reason~~ points to precipitation as the cause, since these two climate types differ ~~essentially by~~ mainly in the amount of precipitation. This result is consistent with the known precipitation bias of the ECHAM5 climate model (see Figure 7 in Stevens et al. (2013)). Both, EMAC and EUMETSAT ~~underestimates the GLEAM global~~ underestimate the global GLEAM *ET* ~~where, however,~~, with more than 50 ~~% of the mismatch occurs~~ % of the discrepancy occurring outside the EUMETSAT region. The difference cannot always be considered to be within the model variability of 20 ~~% due to~~ %. As possible reason for the large variability we propose the model net radiation ~~depending~~ which depends on the choice of forcing data (Badgley et al., 2015). One reason for the underestimation is ~~likely~~ probably the neglect of ~~diffuse radiation impact~~ the effect of diffuse radiation in big-leaf models, as used here~~, enhancing~~. Including diffuse radiation would increase photosynthesis and evapotranspiration (Wang et al., 2022; Knohl and Baldocchi, 2008). Furthermore, ~~representing also~~ the representation of deep plant roots would ensure a more realistic ~~water holding~~ water-holding capacity and avoid ~~a drying out of the soil in the~~ soil desiccation in tropical rainforests (Hagemann and Stacke, 2015).

3.4 Impact on air temperature

The changes in *ET* have ~~significant impacts on~~ a significant effect on the air temperature. Here, we compare the temperature predicted by *REF* to ~~the one~~ that predicted by *LWPfrac*. As expected, ~~from a decrease of~~ a decrease in *ET*, i.e. less cooling, leads to an increase in high daily maximum air temperature values~~increase~~, shown in Figure 6 for warm spells in 2018. We define warm ~~spell conditions~~ spells as a period of at least 3 consecutive days when the daily mean temperature exceeds the 95 ~~%~~ % percentile of the daily mean temperature ~~of~~ for the reference period (1979-2008) (Nairn and Fawcett, 2014). In fact, the difference ~~of~~ between the actual temperature ~~to to~~ and the climatological percentile (~~termed~~ called the 'excess heat factor' in Nairn and Fawcett (2014), which is a measure of intensity of warm ~~spell conditions~~ spells, increases by 1.5K in Europe and 4K in South Africa, in the ~~East U.S.~~ eastern US and the Amazon forest due to the changed ~~plant-water~~ plant water stress function of *LWPfrac*. The global mean air temperature in the lowest model layer (≈ 60m) increases by 2K. ~~Our~~ These results are consistent with recent studies ~~, (e.g., Kala et al., 2016), highlighting~~ (e.g., Seneviratne et al., 2010; Kala et al., 2016), which highlight the role of stomatal stress in the amplification of ~~heatwaves especially affecting the intensity of warm spells and heat waves~~heat waves, especially with respect to their intensity (Barriopedro et al., 2023).

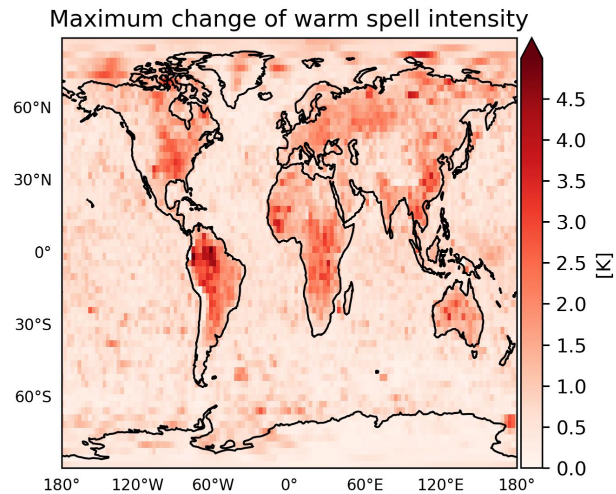

Figure 6. The maximum annual ~~difference~~ change of warm spell intensity (difference of the actual temperature to the climatological percentile) in 2018 due to the plant water stress function.

3.5 Impacts on air pollution

The different representations of plant-water stress affect air pollution mainly by influencing 1) dry deposition fluxes of ozone and 2) meteorological controls on ~~photo-chemistry~~photochemistry. Figure 8 shows the ~~respective changes for~~ effects on tropospheric ozone (O_3) ~~which is a major air pollutant threatening human health as well as the productivity of plants~~when using the *LWPfrac* plant-water stress. Figure 8a shows that the dry deposition of O_3 in *LWPfrac* is ~~decreased~~ reduced by up to 25 ~~%~~%, compared to *REF*, in the tropics and subtropics where dry deposition exerts a strong control on air composition due to high vegetation density. Similar changes apply to precursors with similar characteristics as O_3~~which then~~. This contributes to the increase ~~of~~ in the O_3 mixing ratio (Emmerichs et al., 2021). Furthermore, the reduced *ET* in most vegetated regions exacerbates the atmospheric moisture deficit~~by which the stomata are additionally stressed. The~~, which places additional stress on the stomata. The increased plant water stress leads to a significant temperature increase throughout the tropical regions (see previous section), which is known to favour O_3 production (Pusede et al., 2015). However, the annual mean chemical production and loss terms (Figure 8b,c) are ~~only enhanced~~ increased only in the SW of South America (by up to 10 ~~%) although the increased plant-water stress leads to a significant temperature increase in the entire tropical regions (see previous section)which is known to favour production (Pusede et al., 2015)~~%). The increase ~~of~~ in O_3 production, shown, here follows the increase of OH and HO_2 (HO_x) production~~but it is limited to western Amazon. That is because,~~. Increasing isoprene emissions lead to a linear increase in O_3 since O_3 increases by 0.34 ppb for every 1 ppb increase in formaldehyde (HCHO). HCHO is a direct product of isoprene oxidation with a lifetime of a few hours and is therefore often used as a proxy for isoprene emissions (Palmer et al., 2003). Rapid oxidation reduces the C_5H_8 and increases OH surface concentration in the inner ~~tropical rainforest~~ tropics (Amazon, Congo ~~) the isoprene mixing ratio,~~ Basin) (Fig S1). In the outer tropics, O_3 additionally increases with increasing soil emissions of nitrogen oxides (NO), which is an important O_3 precursor ~~, decreases (Figure S1b) due to increased loss by hydroxyl radical () although isoprene emissionsare enhanced by higher temperatures (Guenther et al., 2006)~~ source in remote regions (far from anthropogenic emissions). The change ~~of the~~ in O_3 loss ~~has~~ is of the same magnitude but ~~is~~ more widespread than the change ~~of the~~ in O_3 production, driven by a relative acceleration of NO_x and HO_x chemistry. These effects then lead to an increase ~~of the~~ in net O_3 loss in the Amazon ~~basin~~ Basin which is overcompensated by ~~the decreased~~ a decrease in O_3 uptake by vegetation. Thus, the annual mean surface O_3 ~~is increased~~ in the tropics and subtropics is increased by up to 10 ~~%~~ % (Figure 8d). This ~~enhances the~~ increases the global tropospheric O_3 burden by 5 Tg per year.

The changes discussed here do not include the O_3 damage to plants, i.e. the biosphere-atmosphere exchange. However, from experiments by e.g. Sadiq et al. (2017) we can learn that an implementation of this response amplifies the O_3-vegetation feedback. Because the caused O_3-increase damages increasingly the plant cells and limits the activity. This further reduces the transpiration and dry deposition which in turn increases O_3 levels. No clear feedback was found for isoprene emissions. Reduced ecosystem production makes only a small contribution to the overall feedback.

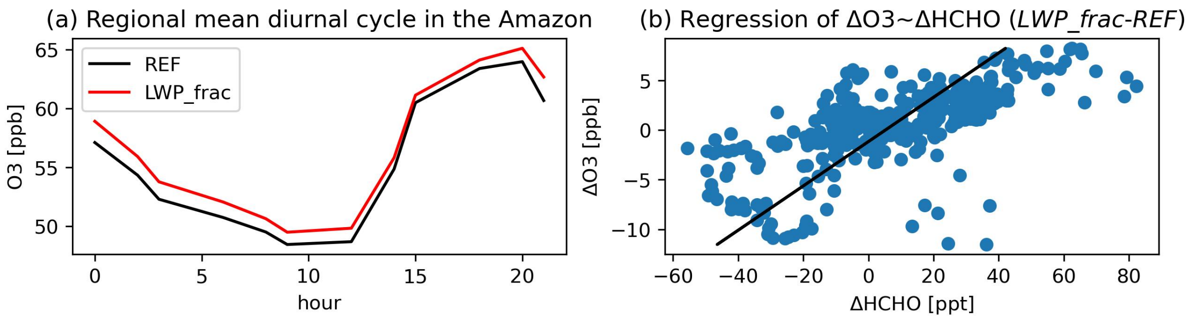

Figure 7. (a) Regional mean diurnal cycle of O_3 in the Amazon (Monsoon region, definition in Fig. 3) and (b) linear regression of the absolute difference (*LWPfrac-REF*] formaldehyde (HCHO) with O_3 surface levels at the ATTO (Amazon Tall Tower Observatory) site in November 2018 (dry season).

3.6 Future scenario

A simulation with the double CO_2 concentration (*futureLWPfrac*) was performed to investigate the role of the new ~~plant-water~~ plant water stress factor in future climate conditions. ~~Besides~~ In addition to perturbing the energy balance at the top of the atmosphere, CO_2 affects the ~~plant sensitivity~~ sensitivity of plants to water stress in our simulations. ~~Increasing~~ An increase in CO_2 has a ~~two-fold impact on the plants~~ two effects on plant behaviour. While it leads to an increased photosynthetic activity, the stomatal conductance is reduced by an average of 40 ~~%~~ % (g_s, Figure 9a). Vicente-Serrano et al. (2022) reports a decrease of 22 ~~%~~ % in stomatal conductance (on average) ~~in stomatal conductance~~ from multiple experiments by doubling only CO_2. We ~~also can~~ can also confirm these findings for equatorial and tropical forests in our simulation. ~~The~~ Due to the dominant decrease in g_s as also reported by Vicente-Serrano et al. (2022), plant transpiration of plants decreases in response to increasing CO_2 in these regions~~due to the dominant decrease of g_s as reported by Vicente-Serrano et al. (2022)~~. In our simulations, however, the impact of the future conditions on g_s is more widespread~~since the changed climatic conditions reduce the~~, as the increased CO_2 also reduces relative humidity almost ~~world-wide and thus stress the~~ worldwide, thus stressing plants. The ~~decrease of~~ 30 % decrease in g_s ~~by 30 % linked to the new plant-water~~ associated with the new plant water stress function is ~~strengthened~~ amplified by the enhanced CO_2. However, this dominates the *ET* only on a daily basis, while the annual sum increases by 30-100~~mm yr^{-1}~~ $mm\,yr^{-1}$ in response to an increased evaporative demand. As a consequence, the 2m temperature ~~is almost doubled~~ almost doubles (Figure 9b) and the relative humidity ~~drops~~ decreases (not shown). These changes are ~~linked to~~ associated with the 20-50 ~~% increase of~~ % increase in solar irradiation (correlation) due to ~~less low-level~~ fewer low level clouds. Pollard and Thompson (1995) also reports ~~on conducting~~ from a doubling CO_2 scenario ~~leading~~ which leads to an increase in stomatal conductance, temperature and specific humidity~~which reduces~~, and thus to a decrease in relative humidity and cloudiness. ECHAM/MESSy does not simulate an interactive carbon cycle, namely the photosynthesis i.e. the net assimilation of CO_2 is calculated to simulate the stomatal conductance with a first-order dependence scaled by the CO_2 deficit between plant cavity and the atmosphere. Several studies have reported that an increase of atmospheric CO_2

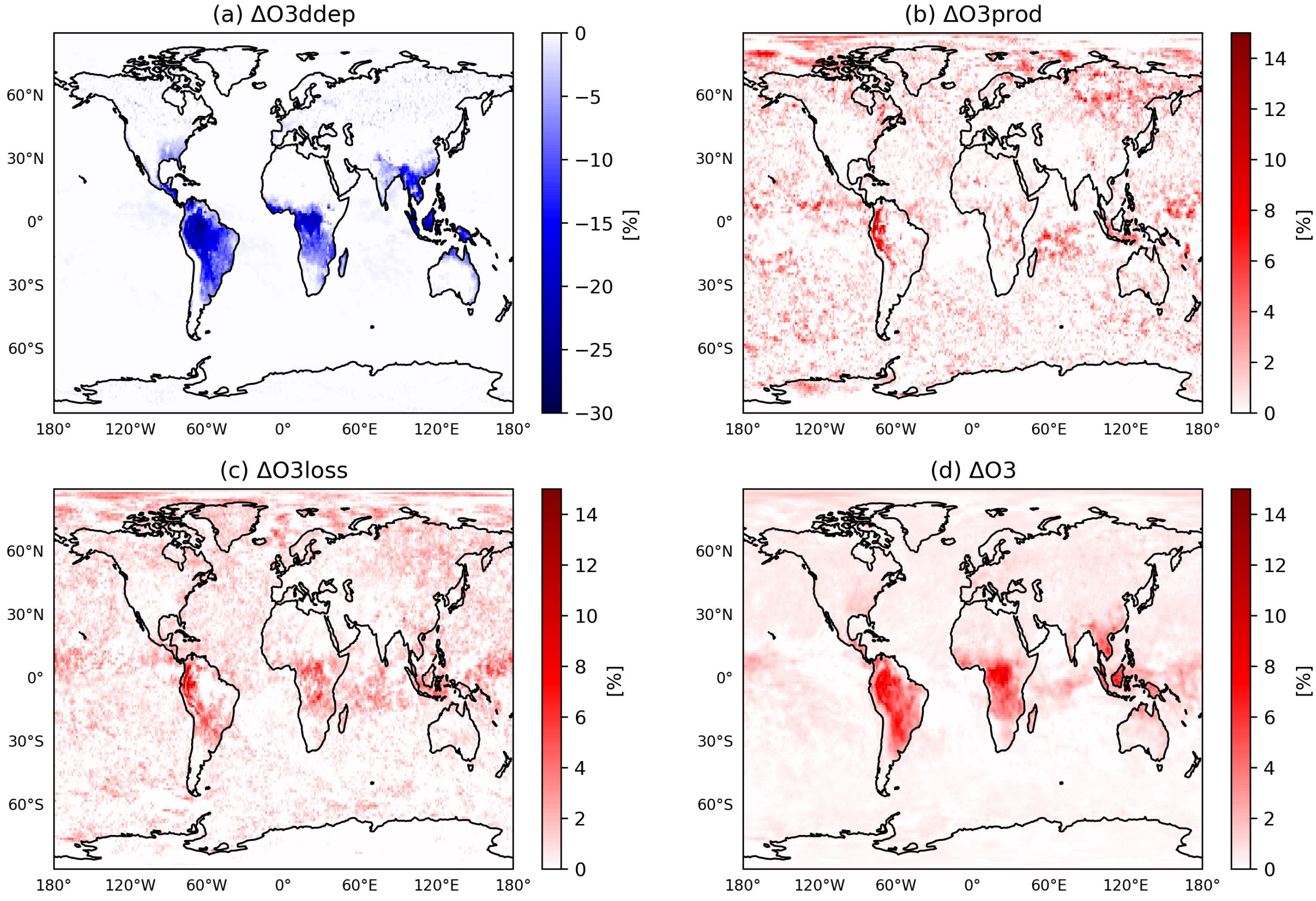

Figure 8. The relative change between *LWPfrac* and *REF* of the annual mean ~~of~~ (a) O_3 dry deposition, (b) chemical O_3 production, (c) chemical loss and (d) surface O_3 mixing ratio.

reduces the leaf stomatal conductance varying by 50 % in dense meadows, by 15 % in decidious forests, and by less than 10 % in coniferous forests. This response is non-linear because the CO_2 stimulation of photosynthesis saturates at high atmospheric CO_2. (Vicente-Serrano et al. (2022) and references therein). Nevertheless, to assess the overall climatic impact of the multiple interactions between terrestrial vegetation and CO_2~~also~~ , the changing vegetation would also have to be ~~considered~~taken in account. However, such an assessment is far more complex and highly uncertain (Vicente-Serrano et al., 2022).

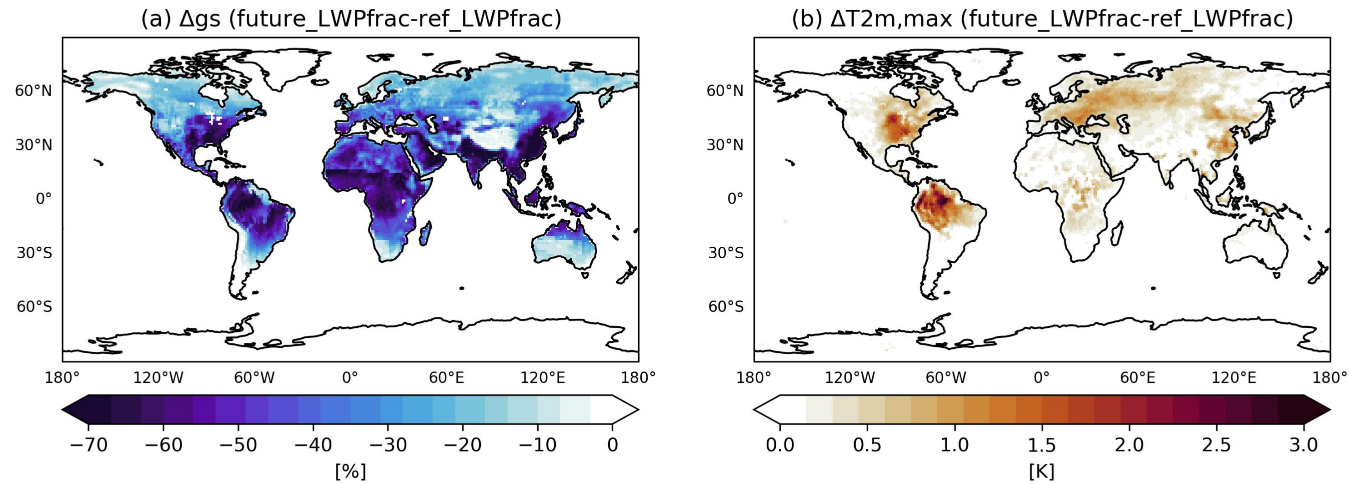

Figure 9. (Boreal) Summer mean change of stomatal conductance (a) and daily 2m maximum temperature (b) when comparing *LWPfrac* ~~in~~ for normal and future conditions (2xCO_2.

4 General discussion

4.1 Default model ~~parametrization~~parametrisation

In models, *ET* is estimated ~~either by the physically-based~~ using either the physically based Penman-Monteith (PM) approach (~~state-of-the-art~~state of the art) or the empirical Priestley-Taylor (PT) equation. The latter ~~one~~ (used in GLEAM) assumes that *ET* ~~only depends~~ depends only on solar radiation and temperature, neglecting wind speed, relative humidity and vapour pressure deficit. ~~But~~ However, because of the link ~~to~~ with air temperature, estimates ~~by~~ from the PT approach show a high correlation ~~to~~ with values estimated by the PM equation~~expect~~, which are expected in dry conditions and in areas with relatively high wind speed (Utset et al., 2004). The key variable for the common ~~parametrization of the~~ parameterisation of plant water stress in plants is the soil moisture, which is described in EMAC by the simplistic but conventional bucket model. A bucket model has ~~been used e.g.~~ long been used, for example, in the JSBACH (Jena Scheme for Biosphere Atmosphere Coupling in Hamburg version) land surface model for a ~~long-time~~ long time (Boone et al., 2004). The inclusion of the surface resistance term in EMAC as ~~the~~ a so-called "~~second-generation models~~second generation model" ~~yields~~ allows a better comparison of estimated evapotranspiration rates with observations than ~~utilizing 'pure'~~ the use of "pure" bucket models (Sellers et al., 1997). However, the lack of soil water holding capacity in the (shallow, one-layer) bucket model leads to an immediate ~~remove~~ removal of water and thus to an unrealistically low soil water in areas with deep roots e.g. tropical forests (Hagemann and Stacke, 2015), despite the thickness of the subsurface layers. Nevertheless, the multi-model evaluation by Robock et al. (1998) found no significant improvements of sophisticated soil models with multiple layers and even vegetation dynamics ~~like~~ such as the CLM or NOAH-LSM over the bucket scheme. More recently, Dong et al. (2022) concluded that most CMIP6 models simulate a warm bias in mid-latitude summer ~~because of incorrect partitioning~~ due to incorrect partitioning of *ET* in canopy transpiration and soil evaporation due to a shallow soil. ~~Moreover~~In addition, even small differences ~~of~~ in the input field capacity data can have large effects on the simulated *ET* (Hagemann and Stacke, 2015).

4.2 More sophisticated models, remaining uncertainties and future recommendations

Boone et al. (2004) shows that sophisticated land surface models (LSMs) ~~agree with each other regarding~~ generally agree with respect to latent heat flux and total runoff. ~~Nevertheless~~However, we note that ~~comparing different LSMs~~ it is very difficult ~~because of the different~~ to compare different LSMs because of differences in model components, ~~parameterizations~~parameterisation, and choice of associated parameters. ~~Also~~In addition, many LSMs only represent shallow ~~soil with a depth down to maximum~~ soils with a maximum depth of 2m (Pan et al., 2020) and therefore cannot account for the storage capacity of ~~the soil~~ soils in the tropical forests as shown by Hagemann and Stacke (2015). ~~For the second-generation~~ The second generation LSMs Pitman (2003), which calculate transpiration and soil moisture ~~across~~ over multiple layers, ~~the predicted soil moisture is somewhat better than with~~ predict soil moisture slightly better than the bucket model. However, ~~when compared to observations,~~ LSMs show a ~~large spread in performance~~ wide range in performance compared to observations (Shao and Henderson-Sellers, 1996). This is certainly due to, but not limited to, the use of different schemes for simulating surface fluxes and soil moisture. ~~Generally, the needed~~ In general, the required spin-up time ~~by~~ of LSMs with deep soil schemes is often not affordable, especially for climate simulations. ~~Using in addition a groundwater model ((e.g., Kollet and Maxwell, 2008))~~ The use of an additional groundwater model (e.g., Jiang et al.; Kollet and Maxwell, 2008; Lam et al.; Larsen et al.) can improve the simulation of the water ~~budget and the groundwater-land surface~~ balance and the groundwater-land-surface interactions (Rahman et al., 2014) but ~~strongly increase~~ greatly increases the required computational resources.

The ~~most recent~~ latest model intercomparison CMIP6 shows on average an ~~overestimated~~ overestimationc of *ET* by the models compared to an observational dataset. However, the CMIP6 ensemble mean underestimates *ET* in regions of high evapotranspiration, such as in the Amazon basin, central Africa, and southeast Asia~~but overestimates *ET* in~~. In regions with low evapotranspiration, such as the Sahara desert, the Middle East, southwest Australia, and the Andes Mountains the models overestimate *ET* (Wang et al., 2021). A multi-model comparison ~~by~~ of *ET* estimates by Pan et al. (2020) shows that the uncertainty is ~~largest~~ greatest in the Amazon basin~~, where~~. There, the standard deviation of the LSM estimates is more than ~~2 times larger than~~ twice that of benchmark estimates. The potential source of uncertainty is the root water uptake. ~~Also, the model~~ Model representation of LAI dynamics or ~~water movement in the soil might cause~~ soil water movement could also contribute to this uncertainty (Pan et al., 2020). In arid and ~~semiarid~~ semi-arid areas, precipitation is a ~~key uncertainty factor for estimates of evapotranspiration~~ major source of uncertainty in evapotranspiration estimates (Pan et al., 2020).

5 Conclusions

We have investigated the ~~significance of plant-water~~ importance of plant water stress for the predictions ~~of~~ for the ground-level ozone concentrations in a warm(er) world. This study has focused on ~~the improvement and assessment of~~ improving and evaluating the evapotranspiration simulated by the atmospheric chemistry model EMAC. We confirm that evapotranspiration is a key process driving the moisture ~~cycling~~ cycle in the atmosphere~~affecting~~ , which affects the global distribution of temperature and warm spell intensity. We also find that ~~plant-water~~ plant water stress has a significant impact on the ~~photo-chemistry and uptake of trace gases~~ photochemistry and trace gas uptake by vegetation. ~~For that~~To do this, we have applied ~~multiple~~ several plant-water stress factors ~~, which~~ that strongly reduce stomatal activity ~~, and have assessed the impacts~~ and assessed the effects at local and global scales. Specifically, we find that:

- The EMAC model represents the spatial variability of transpiration reasonably well
- The global estimates of transpiration are within the literature range~~whereas~~ , while a simple exponential dependence on leaf water ~~dependence~~ potential (*LWPexp*) ~~induces~~ leads a too strong reduction
- The use of stress factors based on leaf water potential ~~lowers~~ reduces the amplitude of the ~~transpiration diurnal cycle but strengthens the model sensitivity~~ diurnal cycle of transpiration but increases the sensitivity of the model to temperature
- The *E/T* partitioning is generally well simulated by EMAC, but in regions ~~like the East U.S.~~ such as the eastern USA the T/ET ratio is too low, probably due to the dry model bias

Close to pollution sources, tropospheric ozone is ~~projected~~ predicted to increase in the future as ~~consequence~~ result of the climate warming. This is often referred to as the 'ozone-climate penalty' (Rasmussen et al., 2013). However, a recent multi-model projection suggests a climate benefit on a global average~~(Zanis et al., 2022). As many uncertainties remain, a recent analysis call~~ , i.e. a decrease in ozone as a consequence of global warming (Zanis et al., 2022). This calls for a re-examination of the link between extreme events and ground-level ozone as many uncertainties remain (Fu and Tian, 2019). Our results highlight the importance of evapotranspiration and ~~plant-water stress for the predictions of~~ plant water stress in predicting air pollution during heat waves and droughts. These extreme events ~~are projected to be~~ will become more frequent and intense (Domeisen et al., 2022). The magnitude of the effects assessed in this study ~~are~~ is model-specific. Nevertheless, ~~they provide a~~ our results provide general guidance for ~~assessment~~ the evaluation and improvement of atmospheric chemistry models, without a state-of-the-art description of land surface processes and a dynamic vegetation model.

Code and data availability. The Modular Earth Submodel System (MESSy) is continuously further developed and applied by a consortium of institutions. The usage of MESSy and access to the source code is licensed to all affiliates of institutions which are members of the MESSy Consortium. Institutions can become a member of the MESSy Consortium by signing the MESSy Memorandum of Understanding. More information can be found on the MESSy Consortium Website http://www.messy-interface.org. The code used in this study is included in the current devel branch of the MESSy repository. The simulation results are archived at the Jülich Supercomputing Centre (JSC) and are available on request. The EUMETSAT *ET* data is available from the website of the EUMETSAT land surface analysis (LSA SAF) consortium (https://landsaf.ipma.pt/ChangeSystemProdLong.do?system=LandSAF+MSG&algo=DMET. The GLEAM data can be provided by a registered user via a ftp server (https://www.gleam.eu/#downloads, last access: 24.07.2023). The TROPOSIF data can be downloaded at http://ftp.sron.nl/open-access-data-2/TROPOMI/tropomi/sif/v2.1/l2b/ (NOVELTI et al., 2021; Guanter et al., 2015).

Author contributions. All authors designed and frequently discussed the concept of the study, TE implemented the code changes supported by DT and Y-SL. The simulations, the data processing and the data analysis were done by TE. All authors wrote and reviewed the manuscript.

Competing interests. The authors declare that they have no conflict of interest.

Acknowledgements. The authors gratefully acknowledge the Gauss Centre for Supercomputing e.V. (www.gauss-centre.eu) for funding this project by providing computing time on the GCS Supercomputer JUWELS (Jülich Supercomputing Centre, 2019) and by the John von Neumann Institute for Computing (NIC) and provided on the supercomputer JURECA (Jülich Supercomputing Centre, 2021) at Jülich Supercomputing Centre (JSC). The authors gratefully acknowledge the Earth System Modelling Project (ESM) for funding this work by providing computing time on the ESM partition of the supercomputer JUWELS at the Jülich Supercomputing Centre (JSC). The EUMETSAT product was provided by the EUMETSAT Satellite Application Facility on Land Surface Analysis (Trigo et al., 2011).The TROPOSIF products were generated by the TROPOSIF team conducted by NOVELTIS under the European Space Agency (ESA) Sentinel-5p+ Innovation activity Contract No 4000127461/19/I-NS (NOVELTI et al., 2021; Guanter et al., 2015). The regridding script was adapted from the work of UWE Raschers group at Forschungszentrum Jülich. This work was supported by funding from the Federal Ministry of Education and Research (BMBF) and the Helmholtz Research Field Earth & Environment for the Innovation Pool Project SCENIC.

References

Product User Manual For Evapotranspiration and Surface Fluxes, https://nextcloud.lsasvcs.ipma.pt/s/r786yz3Ex2Fe9Ya, 2018.

Badgley, G., Fisher, J. B., Jiménez, C., Tu, K. P., and Vinukollu, R.: On Uncertainty in Global Terrestrial Evapotranspiration Estimates from Choice of Input Forcing Datasets, Journal of Hydrometeorology, 16, 1449–1455, https://doi.org/10.1175/JHM-D-14-0040.1, publisher: American Meteorological Society Section: Journal of Hydrometeorology, 2015.

Barriopedro, D., García-Herrera, R., Ordonez, C., Miralles, D. G., and Salcedo-Sanz, S.: Heat Waves: Physical Understanding and Scientific Challenges, Reviews of Geophysics, 61, e2022RG000 780, https://doi.org/10.1029/2022RG000780, _eprint: https://onlinelibrary.wiley.com/doi/pdf/10.1029/2022RG000780, 2023.

Boone, A., Habets, F., Noilhan, J., Clark, D., Dirmeyer, P., Fox, S., Gusev, Y., Haddeland, I., Koster, R., Lohmann, D., Mahanama, S., Mitchell, K., Nasonova, O., Niu, G.-Y., Pitman, A., Polcher, J., Shmakin, A. B., Tanaka, K., van den Hurk, B., Vérant, S., Verseghy, D., Viterbo, P., and Yang, Z.-L.: The Rhône-Aggregation Land Surface Scheme Intercomparison Project: An Overview, J. Climate, 17, 187–208, https://doi.org/10.1175/1520-0442(2004)017<0187:trlssi>2.0.co;2, 2004.

Calvet, J.-C.: Investigating soil and atmospheric plant water stress using physiological and micrometeorological data, Agricultural and Forest Meteorology, 103, 229–247, https://doi.org/10.1016/S0168-1923(00)00130-1, 2000.

Calvet, J.-C., Noilhan, J., Roujean, J.-L., Bessemoulin, P., Cabelguenne, M., Olioso, A., and Wigneron, J.-P.: An interactive vegetation SVAT model tested against data from six contrasting sites, Agricultural and Forest Meteorology, 92, 73–95, https://doi.org/10.1016/S0168-1923(98)00091-4, 1998.

Calvet, J.-C., Rivalland, V., Picon-Cochard, C., and Guehl, J.-M.: Modelling forest transpiration and CO2 fluxes—response to soil moisture stress, Agricultural and Forest Meteorology, 124, 143–156, https://doi.org/10.1016/j.agrformet.2004.01.007, 2004.

Cao, R., Huang, H., Wu, G., Han, D., Jiang, Z., Di, K., and Hu, Z.: Spatiotemporal variations in the ratio of transpiration to evapotranspiration and its controlling factors across terrestrial biomes, Agricultural and Forest Meteorology, 321, 108 984, https://doi.org/10.1016/j.agrformet.2022.108984, 2022.

De Kauwe, M. G., Medlyn, B. E., Zaehle, S., Walker, A. P., Dietze, M. C., Hickler, T., Jain, A. K., Luo, Y., Parton, W. J., Prentice, I. C., Smith, B., Thornton, P. E., Wang, S., Wang, Y.-P., Wårlind, D., Weng, E., Crous, K. Y., Ellsworth, D. S., Hanson, P. J., Seok Kim, H., Warren, J. M., Oren, R., and Norby, R. J.: Forest water use and water use efficiency at elevated CO2: a model-data intercomparison at two contrasting temperate forest FACE sites, Global Change Biology, 19, 1759–1779, https://doi.org/10.1111/gcb.12164, _eprint: https://onlinelibrary.wiley.com/doi/pdf/10.1111/gcb.12164, 2013.

Delworth, T. L. and Manabe, S.: The influence of potential evaporation on the variabilities of simulated soil wetness and climate, Journal of Climate, 1, 523–547, 1988.

Domeisen, D. I. V., Eltahir, E. A. B., Fischer, E. M., Knutti, R., Perkins-Kirkpatrick, S. E., Schär, C., Seneviratne, S. I., Weisheimer, A., and Wernli, H.: Prediction and projection of heatwaves, Nature Reviews Earth & Environment, https://doi.org/10.1038/s43017-022-00371-z, publisher: Nature Publishing Group, 2022.

Dong, J., Lei, F., and Crow, W. T.: Land transpiration-evaporation partitioning errors responsible for modeled summertime warm bias in the central United States, Nature Communications, 13, 336, https://doi.org/10.1038/s41467-021-27938-6, number: 1 Publisher: Nature Publishing Group, 2022.

Drake, J. E., Tjoelker, M. G., Vårhammar, A., Medlyn, B. E., Reich, P. B., Leigh, A., Pfautsch, S., Blackman, C. J., López, R., Aspinwall, M. J., Crous, K. Y., Duursma, R. A., Kumarathunge, D., De Kauwe, M. G., Jiang, M., Nicotra, A. B., Tissue, D. T., Choat, B., Atkin, O. K., and Barton, C. V. M.: Trees tolerate an extreme heatwave via sustained transpirational cooling and increased leaf thermal tolerance, Global Change Biology, 24, 2390–2402, https://doi.org/10.1111/gcb.14037, _eprint: https://onlinelibrary.wiley.com/doi/pdf/10.1111/gcb.14037, 2018.

ECMWF: IFS Documentation CY47R3, IFS Documentation, ECMWF, 2021.

Egea, G., Verhoef, A., and Vidale, P. L.: Towards an improved and more flexible representation of water stress in coupled photosynthesis–stomatal conductance models, Agricultural and Forest Meteorology, 151, 1370–1384, https://doi.org/10.1016/j.agrformet.2011.05.019, 2011.

Elnashar, A., Wang, L., Wu, B., Zhu, W., and Zeng, H.: Synthesis of global actual evapotranspiration from 1982 to 2019, Earth System Science Data, 13, 447–480, https://doi.org/10.5194/essd-13-447-2021, publisher: Copernicus GmbH, 2021.

Emmerichs, T., Kerkweg, A., Ouwersloot, H., Fares, S., Mammarella, I., and Taraborrelli, D.: A revised dry deposition scheme for land–atmosphere exchange of trace gases in ECHAM/MESSy v2.54, Geoscientific Model Development, 14, 495–519, https://doi.org/10.5194/gmd-14-495-2021, publisher: Copernicus GmbH, 2021.

Forzieri, G., Miralles, D. G., Ciais, P., Alkama, R., Ryu, Y., Duveiller, G., Zhang, K., Robertson, E., Kautz, M., Martens, B., Jiang, C., Arneth, A., Georgievski, G., Li, W., Ceccherini, G., Anthoni, P., Lawrence, P., Wiltshire, A., Pongratz, J., Piao, S., Sitch, S., Goll, D. S., Arora, V. K., Lienert, S., Lombardozzi, D., Kato, E., Nabel, J. E. M. S., Tian, H., Friedlingstein, P., and Cescatti, A.: Increased control of vegetation on global terrestrial energy fluxes, Nature Climate Change, 10, 356–362, https://doi.org/10.1038/s41558-020-0717-0, number: 4 Publisher: Nature Publishing Group, 2020.

Fu, T.-M. and Tian, H.: Climate Change Penalty to Ozone Air Quality: Review of Current Understandings and Knowledge Gaps, Current Pollution Reports, 5, 159–171, https://doi.org/10.1007/s40726-019-00115-6, 2019.

Giorgetta, M. A., Roeckner, E., Mauritsen, T., Bader, J., Crueger, T., Esch, M., Rast, S., Kornblueh, L., Schmidt, H., Kinne, S., Hohenegger, C., Möbis, B., Krismer, T., Wieners, H., and Stevens, B.: The atmospheric general circulation model ECHAM6: Model description, Reports on Earth System Science, p. 177, 2013.

Guanter, L., Bacour, C., Schneider, A., Aben, I., van Kempen, T. A., Maignan, F., Retscher, C., Köhler, P., Frankenberg, C., J., and J., Zhang, Y.: The TROPOSIF global sun-induced fluorescence dataset from the Sentinel-5P TROPOMI mission, Earth System Science Data, https://doi.org/https://doi.org/10.5194/essd-2021-199, 2015.

Guenther, A., Karl, T., Harley, P., Wiedinmyer, C., Palmer, P. I., and Geron, C.: Estimates of global terrestrial isoprene emissions using MEGAN (Model of Emissions of Gases and Aerosols from Nature), Atmospheric Chemistry and Physics, 6, 3181–3210, https://doi.org/10.5194/acp-6-3181-2006, 2006.

Hagemann, S.: An Improved Land Surface Parameter Dataset for Global and Regional Climate Models, Tech. Rep., 336, https://doi.org/10.17617/2.2344576, 2002.

Hagemann, S. and Stacke, T.: Impact of the soil hydrology scheme on simulated soil moisture memory, Climate Dynamics, 44, 1731–1750, https://doi.org/10.1007/s00382-014-2221-6, publisher: Springer, 2015.

Harper, A. B., Williams, K. E., McGuire, P. C., Duran Rojas, M. C., Hemming, D., Verhoef, A., Huntingford, C., Rowland, L., Marthews, T., Breder Eller, C., Mathison, C., Nobrega, R. L. B., Gedney, N., Vidale, P. L., Otu-Larbi, F., Pandey, D., Garrigues, S., Wright, A., Slevin, D., De Kauwe, M. G., Blyth, E., Ardö, J., Black, A., Bonal, D., Buchmann, N., Burban, B., Fuchs, K., de Grandcourt, A., Mammarella, I., Merbold, L., Montagnani, L., Nouvellon, Y., Restrepo-Coupe, N., and Wohlfahrt, G.: Improvement of modeling plant responses to low soil moisture in JULESvn4.9 and evaluation against flux tower measurements, Geoscientific Model Development, 14, 3269–3294, https://doi.org/10.5194/gmd-14-3269-2021, 2021.

Iturbide, M., Gutiérrez, J. M., Alves, L. M., Bedia, J., Cerezo-Mota, R., Cimadevilla, E., Cofiño, A. S., Di Luca, A., Faria, S. H., Gorodetskaya, I. V., Hauser, M., Herrera, S., Hennessy, K., Hewitt, H. T., Jones, R. G., Krakovska, S., Manzanas, R., Martínez-Castro, D., Narisma, G. T., Nurhati, I. S., Pinto, I., Seneviratne, S. I., van den Hurk, B., and Vera, C. S.: An update of IPCC climate reference regions for subcontinental analysis of climate model data: definition and aggregated datasets, Earth System Science Data, 12, 2959–2970, https://doi.org/10.5194/essd-12-2959-2020, 2020.

Jacobs, C. M. J.: Stomata1 behaviour and photosynthetic rate of unstressed grapevines in semi-arid conditions, AGRICULTURAL AND FOREST METEOROLOGY, p. 24, 1994.

Jiang, X., Niu, G.-Y., and Yang, Z.-L.: Impacts of vegetation and groundwater dynamics on warm season precipitation over the Central United States, 114, D06 109, http://dx.doi.org/10.1029/2008JD010756.

Jülich Supercomputing Centre: JUWELS: Modular Tier-0/1 Supercomputer at the Jülich Supercomputing Centre, Journal of large-scale research facilities, 5, https://doi.org/10.17815/jlsrf-5-171, 2019.

Jülich Supercomputing Centre: JURECA: Data Centric and Booster Modules implementing the Modular Supercomputing Architecture at Jülich Supercomputing Centre, Journal of large-scale research facilities, 7, https://doi.org/10.17815/jlsrf-7-182, 2021.

Jöckel, P., Kerkweg, A., Pozzer, A., Sander, R., Tost, H., Riede, H., Baumgaertner, A., Gromov, S., and Kern, B.: Development cycle 2 of the Modular Earth Submodel System (MESSy2), Geoscientific Model Development, 3, 717–752, https://doi.org/10.5194/gmd-3-717-2010, publisher: Copernicus GmbH, 2010.

Jöckel, P., Tost, H., Pozzer, A., Kunze, M., Kirner, O., Brenninkmeijer, C. A. M., Brinkop, S., Cai, D. S., Dyroff, C., Eckstein, J., Frank, F., Garny, H., Gottschaldt, K.-D., Graf, P., Grewe, V., Kerkweg, A., Kern, B., Matthes, S., Mertens, M., Meul, S., Neumaier, M., Nützel, M., Oberländer-Hayn, S., Ruhnke, R., Runde, T., Sander, R., Scharffe, D., and Zahn, A.: Earth System Chemistry integrated Modelling (ESCiMo) with the Modular Earth Submodel System (MESSy) version 2.51, Geoscientific Model Development, 9, 1153–1200, https://doi.org/10.5194/gmd-9-1153-2016, publisher: Copernicus GmbH, 2016.

Kala, J., De Kauwe, M. G., Pitman, A. J., Medlyn, B. E., Wang, Y.-P., Lorenz, R., and Perkins-Kirkpatrick, S. E.: Impact of the representation of stomatal conductance on model projections of heatwave intensity, Scientific reports, 6, 23 418, 2016.

Katul, G. G., Palmroth, S., and Oren, R.: Leaf stomatal responses to vapour pressure deficit under current and CO-enriched atmosphere explained by the economics of gas exchange, Plant, Cell & Environment, 32, 968–979, https://doi.org/10.1111/j.1365-3040.2009.01977.x, publisher: Wiley Online Library, 2009.

Katul, G. G., Oren, R., Manzoni, S., Higgins, C., and Parlange, M. B.: Evapotranspiration: A process driving mass transport and energy exchange in the soil-plant-atmosphere-climate system, Reviews of Geophysics, 50, https://doi.org/10.1029/2011RG000366, _eprint: https://onlinelibrary.wiley.com/doi/pdf/10.1029/2011RG000366, 2012.

Keenan, T., Sabate, S., and Gracia, C.: Soil water stress and coupled photosynthesis–conductance models: Bridging the gap between conflicting reports on the relative roles of stomatal, mesophyll conductance and biochemical limitations to photosynthesis, Agricultural and Forest Meteorology, 150, 443–453, https://doi.org/10.1016/j.agrformet.2010.01.008, 2010.

Kennedy, D., Swenson, S., Oleson, K. W., Lawrence, D. M., Fisher, R., Lola da Costa, A. C., and Gentine, P.: Implementing Plant Hydraulics in the Community Land Model, Version 5, Journal of Advances in Modeling Earth Systems, 11, 485–513, https://doi.org/10.1029/2018MS001500, _eprint: https://onlinelibrary.wiley.com/doi/pdf/10.1029/2018MS001500, 2019.

Kerkweg, A., Buchholz, J., Ganzeveld, L., Pozzer, A., Tost, H., and Jöckel, P.: An implementation of the dry removal processes DRY DEPosition and SEDImentation in the Modular Earth Submodel System (MESSy), Atmospheric Chemistry and Physics, 6, 4617–4632, https://doi.org/10.5194/acp-6-4617-2006, publisher: Copernicus GmbH, 2006.

Klein, T.: The variability of stomatal sensitivity to leaf water potential across tree species indicates a continuum between isohydric and anisohydric behaviours, Functional Ecology, 28, 1313–1320, https://doi.org/10.1111/1365-2435.12289, _eprint: https://onlinelibrary.wiley.com/doi/pdf/10.1111/1365-2435.12289, 2014.

Knohl, A. and Baldocchi, D. D.: Effects of diffuse radiation on canopy gas exchange processes in a forest ecosystem, Journal of Geophysical Research: Biogeosciences, 113, https://doi.org/10.1029/2007JG000663, _eprint: https://onlinelibrary.wiley.com/doi/pdf/10.1029/2007JG000663, 2008.

Kollet, S. J. and Maxwell, R. M.: Capturing the influence of groundwater dynamics on land surface processes using an integrated, distributed watershed model, Water Resour. Res., 44, W02 402, http://dx.doi.org/10.1029/2007WR006004, 2008.

Kozlowski, T. T., Kramer, P. J., and Pallardy, S. G.: The Physiological Ecology of Woody Plants, Tree Physiology, 8, 213, https://doi.org/10.1093/treephys/8.2.213, 1991.

Lam, A., Karssenberg, D., van den Hurk, B. J. J. M., and Bierkens, M. F. P.: Spatial and temporal connections in groundwater contribution to evaporation, 8, 1541–1568, http://www.hydrol-earth-syst-sci-discuss.net/8/1541/2011/.

Larsen, M. A. D., Refsgaard, J. C., Drews, M., Butts, M. B., Jensen, K. H., Christensen, J. H., and Christensen, O. B.: Results from a full coupling of the HIRHAM regional climate model and the MIKE SHE hydrological model for a Danish catchment, 18, 4733–4749, http://www.hydrol-earth-syst-sci.net/18/4733/2014/.

Lian, X., Piao, S., Huntingford, C., Li, Y., Zeng, Z., Wang, X., Ciais, P., McVicar, T. R., Peng, S., Ottlé, C., Yang, H., Yang, Y., Zhang, Y., and Wang, T.: Partitioning global land evapotranspiration using CMIP5 models constrained by observations, Nature Climate Change, 8, 640–646, https://doi.org/10.1038/s41558-018-0207-9, number: 7 Publisher: Nature Publishing Group, 2018.

Maes, W. H., Pagán, B. R., Martens, B., Gentine, P., Guanter, L., Steppe, K., Verhoest, N. E. C., Dorigo, W., Li, X., Xiao, J., and Miralles, D. G.: Sun-induced fluorescence closely linked to ecosystem transpiration as evidenced by satellite data and radiative transfer models, Remote Sensing of Environment, 249, 112 030, https://doi.org/10.1016/j.rse.2020.112030, 2020.

Martini, D., Sakowska, K., Wohlfahrt, G., Pacheco-Labrador, J., van der Tol, C., Porcar-Castell, A., Magney, T. S., Carrara, A., Colombo, R., El-Madany, T. S., Gonzalez-Cascon, R., Martín, M. P., Julitta, T., Moreno, G., Rascher, U., Reichstein, M., Rossini, M., and Migliavacca, M.: Heatwave breaks down the linearity between sun-induced fluorescence and gross primary production, New Phytologist, 233, 2415–2428, https://doi.org/10.1111/nph.17920, _eprint: https://onlinelibrary.wiley.com/doi/pdf/10.1111/nph.17920, 2022.

Millar, A. A., Jensen, R. E., Bauer, A., and Norum, E. B.: Influence of atmospheric and soil environmental parameters on the diurnal fluctuations of leaf water status of barley, Agricultural Meteorology, 8, 93–105, https://doi.org/10.1016/0002-1571(71)90099-9, 1971.

Miralles, D. G., Holmes, T. R. H., De Jeu, R. A. M., Gash, J. H., Meesters, A. G. C. A., and Dolman, A. J.: Global land-surface evaporation estimated from satellite-based observations, Hydrology and Earth System Sciences, 15, 453–469, https://doi.org/10.5194/hess-15-453-2011, 2011.

Miralles, D. G., Gentine, P., Seneviratne, S. I., and Teuling, A. J.: Land-atmospheric feedbacks during droughts and heatwaves: state of the science and current challenges, Annals of the New York Academy of Sciences, 1436, 19–35, https://doi.org/10.1111/nyas.13912, 2019.

Nairn, J. R. and Fawcett, R. J. B.: The excess heat factor: a metric for heatwave intensity and its use in classifying heatwave severity, International Journal of Environmental Research and Public Health, 12, 227–253, https://doi.org/10.3390/ijerph120100227, 2014.

NOVELTI, UPV, SRON, LSCE, and ESA: The TROPOSIF global sun-induced fluorescence dataset from the TROPOMI mission, https://doi.org/https://doi.org/10.5270/esa-s5p_innovation-sif-20180501_20210320- v2.1-202104, 2021.

Palmer, P. I., Jacob, D. J., Fiore, A. M., Martin, R. V., Chance, K., and Kurosu, T. P.: Mapping isoprene emissions over North America using formaldehyde column observations from space, Journal of Geophysical Research: Atmospheres, 108, https://doi.org/https://doi.org/10.1029/2002JD002153, 2003.

Pan, S., Pan, N., Tian, H., Friedlingstein, P., Sitch, S., Shi, H., Arora, V. K., Haverd, V., Jain, A. K., Kato, E., Lienert, S., Lombardozzi, D., Nabel, J. E. M. S., Ottlé, C., Poulter, B., Zaehle, S., and Running, S. W.: Evaluation of global terrestrial evapotranspiration using state-of-the-art approaches in remote sensing, machine learning and land surface modeling, Hydrology and Earth System Sciences, 24, 1485–1509, https://doi.org/10.5194/hess-24-1485-2020, publisher: Copernicus GmbH, 2020.

Paço, T. A. d., Ferreira, M. I., and Pacheco, C. A.: Scheduling peach orchard irrigation in water stress conditions: use of relative transpiration and predawn leaf water potential, Fruits, 68, 147–158, https://doi.org/10.1051/fruits/2013061, 2013.

Pitman, A. J.: The evolution of, and revolution in, land surface schemes designed for climate models, Int. J. Climatol., 23, 479–510, http://dx.doi.org/10.1002/joc.893, 2003.

Pollard, D. and Thompson, S. L.: Use of a land-surface-transfer scheme (LSX) in a global climate model: the response to doubling stomatal resistance, Results from the Model Evaluation Consortium for Climate Assessment, 10, 129–161, http://www.sciencedirect.com/science/article/pii/0921818194000237, 1995.

Pusede, S. E., Steiner, A. L., and Cohen, R. C.: Temperature and Recent Trends in the Chemistry of Continental Surface Ozone, Chemical Reviews, 115, 3898–3918, https://doi.org/10.1021/cr5006815, publisher: American Chemical Society, 2015.

Rahman, M., Sulis, M., and Kollet, S. J.: The concept of dual-boundary forcing in land surface-subsurface interactions of the terrestrial hydrologic and energy cycles, Water Resour. Res., 50, 8531–8548, http://dx.doi.org/10.1002/2014WR015738, 2014.

Rasmussen, D. J., Hu, J., Mahmud, A., and Kleeman, M. J.: The Ozone–Climate Penalty: Past, Present, and Future, Environmental Science & Technology, 47, 14 258–14 266, https://doi.org/10.1021/es403446m, publisher: American Chemical Society, 2013.

Robock, A., Schlosser, C. A., Vinnikov, K. Y., Speranskaya, N. A., Entin, J. K., and Qiu, S.: Evaluation of the AMIP soil moisture simulations, Global and Planetary Change, 19, 181–208, https://doi.org/10.1016/S0921-8181(98)00047-2, 1998.

Roeckner, E., Bäuml, G., Bonaventura, L., Brokopf, R., Esch, M., Giorgetta, M., Hagemann, S., Kirchner, I., Kornblueh, L., Manzini, E., and others: The atmospheric general circulation model ECHAM 5. PART I: Model description, MPI report, publisher: Max-Planck-Institut für Meteorologie, 2003.

Rogers, A., Medlyn, B. E., Dukes, J. S., Bonan, G., von Caemmerer, S., Dietze, M. C., Kattge, J., Leakey, A. D. B., Mercado, L. M., Niinemets, U., Prentice, I. C., Serbin, S. P., Sitch, S., Way, D. A., and Zaehle, S.: A roadmap for improving the representation of photosynthesis in Earth system models, New Phytologist, 213, 22–42, https://doi.org/10.1111/nph.14283, _eprint: https://onlinelibrary.wiley.com/doi/pdf/10.1111/nph.14283, 2017.

Sabot, M. E. B., De Kauwe, M. G., Pitman, A. J., Medlyn, B. E., Ellsworth, D. S., Martin-StPaul, N. K., Wu, J., Choat, B., Limousin, J.-M., Mitchell, P. J., Rogers, A., and Serbin, S. P.: One Stomatal Model to Rule Them All? Toward Improved Representation of Carbon and Water Exchange in Global Models, Journal of Advances in Modeling Earth Systems, 14, e2021MS002 761, https://doi.org/10.1029/2021MS002761, _eprint: https://onlinelibrary.wiley.com/doi/pdf/10.1029/2021MS002761, 2022.

Sadiq, M., Tai, A. P. K., Lombardozzi, D., and Val Martin, M.: Effects of ozone–vegetation coupling on surface ozone air quality via biogeochemical and meteorological feedbacks, Atmospheric Chemistry and Physics, 17, 3055–3066, https://doi.org/10.5194/acp-17-3055-2017, 2017.

Schulz, J.-P., Dümenil, L., and Polcher, J.: On the land surface–atmosphere coupling and its impact in a single-column atmospheric model, Journal of Applied Meteorology, 40, 642–663, https://doi.org/10.1175/1520-0450(2001)040<0642:OTLSAC>2.0.CO;2, 2001.

Sellers, P., Dickinson, R. E., Randall, D., Betts, A., Hall, F., Berry, J., Collatz, G., Denning, A., Mooney, H., Nobre, C., and others: Modeling the exchanges of energy, water, and carbon between continents and the atmosphere, Science, 275, 502–509, publisher: American Association for the Advancement of Science, 1997.

Seneviratne, S. I., Corti, T., Davin, E. L., Hirschi, M., Jaeger, E. B., Lehner, I., Orlowsky, B., and Teuling, A. J.: Investigating soil moisture–climate interactions in a changing climate: A review, Earth-Science Reviews, 99, 125–161, https://doi.org/10.1016/j.earscirev.2010.02.004, 2010.

Shao, Y. and Henderson-Sellers, A.: Modeling soil moisture: A Project for Intercomparison of Land Surface Parameterization Schemes Phase 2(b), J. Geophys. Res., 101, 7227–7250, http://dx.doi.org/10.1029/95JD03275, 1996.

Shepherd, T. G., Boyd, E., Calel, R. A., Chapman, S. C., Dessai, S., Dima-West, I. M., Fowler, H. J., James, R., Maraun, D., Martius, O., and others: Storylines: an alternative approach to representing uncertainty in physical aspects of climate change, Climatic change, 151, 555–571, https://doi.org/10.1007/s10584-018-2317-9, publisher: Springer, 2018.

Stevens, B., Giorgetta, M., Esch, M., Mauritsen, T., Crueger, T., Rast, S., Salzmann, M., Schmidt, H., Bader, J., Block, K., Brokopf, R., Fast, I., Kinne, S., Kornblueh, L., Lohmann, U., Pincus, R., Reichler, T., and Roeckner, E.: Atmospheric component of the MPI-M Earth System Model: ECHAM6, Journal of Advances in Modeling Earth Systems, 5, 146–172, https://doi.org/10.1002/jame.20015, 2013.

Thépaut, J.-N., Dee, D., Engelen, R., and Pinty, B.: The Copernicus programme and its climate change service, in: IGARSS 2018-2018 IEEE International Geoscience and Remote Sensing Symposium, pp. 1591–1593, IEEE, https://doi.org/10.1109/IGARSS.2018.8518067, 2018.

Tost, H., Jöckel, P., Kerkweg, A., Sander, R., and Lelieveld, J.: Technical note: A new comprehensive SCAVenging submodel for global atmospheric chemistry modelling, Atmospheric Chemistry and Physics, 6, 565–574, https://doi.org/10.5194/acp-6-565-2006, 2006.

Trigo, I. F., Dacamara, C. C., Viterbo, P., Roujean, J.-L., Olesen, F., Barroso, C., Camacho-de Coca, F., Carrer, D., Freitas, S. C., Garcia-Haro, J., Geiger, B., Gellens-Meulenberghs, F., Ghilain, N., Melia, J., Pessanha, L., Siljamo, N., and Arboleda, A.: The Satellite Application Facility for Land Surface Analysis, International Journal of Remote Sensing, 32, 2725–2744, https://doi.org/10.1080/01431161003743199, 2011.

Tuzet, A., Perrier, A., and Leuning, R.: A coupled model of stomatal conductance, photosynthesis and transpiration, Plant, Cell & Environment, 26, 1097–1116, https://doi.org/10.1046/j.1365-3040.2003.01035.x, _eprint: https://onlinelibrary.wiley.com/doi/pdf/10.1046/j.1365-3040.2003.01035.x, 2003.

Utset, A., Farre, I., Martinez-Cob, A., and Cavero, J.: Comparing Penman–Monteith and Priestley–Taylor approaches as reference-evapotranspiration inputs for modeling maize water-use under Mediterranean conditions, Agricultural Water Management, 66, 205–219, https://doi.org/10.1016/j.agwat.2003.12.003, 2004.

Verhoef, A. and Egea, G.: Modeling plant transpiration under limited soil water: Comparison of different plant and soil hydraulic parameterizations and preliminary implications for their use in land surface models, Agricultural and Forest Meteorology, 191, 22–32, https://doi.org/10.1016/j.agrformet.2014.02.009, 2014.

Vicente-Serrano, S. M., Miralles, D. G., McDowell, N., Brodribb, T., Domínguez-Castro, F., Leung, R., and Koppa, A.: The uncertain role of rising atmospheric CO2 on global plant transpiration, Earth-Science Reviews, 230, 104 055, https://doi.org/10.1016/j.earscirev.2022.104055, 2022.

Wang, B., Yue, X., Zhou, H., and Zhu, J.: Impact of diffuse radiation on evapotranspiration and its coupling to carbon fluxes at global FLUXNET sites, Agricultural and Forest Meteorology, 322, 109 006, https://doi.org/10.1016/j.agrformet.2022.109006, 2022.

Wang, K. and Dickinson, R. E.: A review of global terrestrial evapotranspiration: Observation, modeling, climatology, and climatic variability, Reviews of Geophysics, 50, https://doi.org/10.1029/2011RG000373, 2012.

Wang, Z., Zhan, C., Ning, L., and Guo, H.: Evaluation of global terrestrial evapotranspiration in CMIP6 models, Theoretical and Applied Climatology, 143, 521–531, https://doi.org/10.1007/s00704-020-03437-4, 2021.

Xiao, J., Fisher, J. B., Hashimoto, H., Ichii, K., and Parazoo, N. C.: Emerging satellite observations for diurnal cycling of ecosystem processes, Nature Plants, 7, 877–887, https://doi.org/10.1038/s41477-021-00952-8, number: 7 Publisher: Nature Publishing Group, 2021.

Xiao, Z., Liang, S., and Jiang, B.: Evaluation of four long time-series global leaf area index products, Agricultural and Forest Meteorology, 246, 218–230, https://doi.org/10.1016/j.agrformet.2017.06.016, publisher: Elsevier, 2017.

Zanis, P., Akritidis, D., Turnock, S., Naik, V., Szopa, S., Georgoulias, A. K., Bauer, S. E., Deushi, M., Horowitz, L. W., Keeble, J., Sager, P. L., O'Connor, F. M., Oshima, N., Tsigaridis, K., and Noije, T. v.: Climate change penalty and benefit on surface ozone: a global perspective based on CMIP6 earth system models, Environmental Research Letters, 17, 024 014, https://doi.org/10.1088/1748-9326/ac4a34, publisher: IOP Publishing, 2022.

Zhang, L., Brook, J., and Vet, R.: A revised parameterization for gaseous dry deposition in air-quality models, Atmospheric Chemistry and Physics, 3, 2067–2082, publisher: Copernicus GmbH, 2003.

Zhang, Y., Chiew, F. H. S., Peña-Arancibia, J., Sun, F., Li, H., and Leuning, R.: Global variation of transpiration and soil evaporation and the role of their major climate drivers, Journal of Geophysical Research: Atmospheres, 122, 6868–6881, https://doi.org/10.1002/2017JD027025, _eprint: https://onlinelibrary.wiley.com/doi/pdf/10.1002/2017JD027025, 2017.

Zhou, S., Duursma, R. A., Medlyn, B. E., Kelly, J. W. G., and Prentice, I. C.: How should we model plant responses to drought? An analysis of stomatal and non-stomatal responses to water stress, Agricultural and Forest Meteorology, 182-183, 204–214, https://doi.org/10.1016/j.agrformet.2013.05.009, 2013.